

# Measurement dependence in a Bell inequality arising from the dynamics of hidden variables

Sophia M. Walls and Ian J. Ford\*

*Department of Physics and Astronomy, University College London,  
Gower Street, London, WC1E 6BT, United Kingdom*

Bell inequalities rely on an assumption that the probabilities of adopting configurations of hidden variables describing a system prior to measurement are independent of the choice of measured physical property, also known as measurement independence. Weakening this assumption could alter the inequalities to accommodate experimental data whilst maintaining local interactions. A natural avenue for achieving this would be to model measurement as a dynamical process involving an interaction between the system and its environment (the measurement apparatus), that drives the hidden variables towards attractors representing measurement outcomes of the observable. Implementing such hidden variable dynamics, we can infer from observed correlations the hidden variable probability distributions before measurement, which differ according to which measurement settings were chosen. We explore various models of the dynamics of the hidden variables under measurement, revealing features that can create measurement dependence and others that can not.

## I. INTRODUCTION

Bell inequalities arise from analysis of the statistics of purported ‘hidden variables’ that evolve according to local interactions and represent ‘elements of reality’ with definite values prior to measurement. It has been demonstrated that the inequalities can be violated, with recent experiments removing areas of uncertainty in the analysis such as the fair-sampling and locality loopholes [1–7]. The implication is either that physical effects operate non-locally between space-like separated points, or that we have to abandon the concept of a reality independent of observation at microscopic scales [8, 9].

Should we wish to avoid these conclusions it is necessary to examine the assumptions made in Bell’s analysis, one of which is ‘measurement independence’ [10], according to which the probabilities of adopting certain configurations of the hidden variables prior to measurement are independent of the measurement settings. We examine the effect of relaxing this assumption in the standard situation where two spin half particles in an entangled singlet state have spin components separately measured along arbitrarily chosen axes  $\hat{n}_1$  and  $\hat{n}_2$ . We demonstrate, by introducing measurement dependence, that the upper bound of the Clauser-Horne-Shimony-Holt (CHSH) parameter may be increased.

The system prior to measurement is specified by a set of hidden variables  $\lambda$  adopted according to a probability density function (pdf)  $\rho(\lambda)$ . The assumption of measurement independence is the use in the analysis of a pdf that depends neither on the measurement axes  $\hat{n}_1, \hat{n}_2$  nor the measurement outcome. This can seem reasonable but it does not necessarily follow if measurement is a dynamical process.

The classical acquisition of information is taken to occur without changing the system state, while in quan-

tum mechanics the initial state encodes properties that are extracted with instantaneous projection of the system to one of the eigenstates of the measured property. We consider here that measurement could instead involve the nonlinear evolution of hidden variables towards attractors in their phase space that correspond to system eigenstates (and device readings correlated with those eigenstates). The evolution could be deterministic or stochastic. The point is that dynamics would create a relationship between final outcomes, represented by an ensemble of post-measurement states described by hidden variables residing at measurement setting-dependent attractors in the phase space, and initial states represented by an ensemble of hidden variable configurations prior to measurement.

The probability distribution of hidden variables before measurement could therefore differ according to the chosen measurement setting. In this paper we study the potential for such a mechanism to account for quantum correlations that break the Bell bound.

Violation of measurement independence is important since it has the potential to render vulnerable to attack any entanglement-based technologies that rely on true quantum randomness [11–23]. The effect of measurement dependence on the upper bound of the CHSH parameter has been explored before [24–35], with recent advances demonstrating that violations of the CHSH may be reproduced without removing all freedom of choice in settings [27, 30, 35]. Experimental advances have also been made in an attempt to close the ‘measurement-dependence loophole’ by allowing measurement settings to be chosen by random or spatio-temporally distant influences [36–40]. We nonetheless take the view that the settings, however they are chosen, can provide information about the system variables prior to measurement, when the process of measurement is dynamical. The question is then not *how* the measurement settings are chosen but *how much* such settings can yield information about the possible distribution of the system variables

\* Correspondence to: sophia.walls.17@ucl.ac.uk

prior to measurement. Such information can then enable an *inference* to be made regarding the probability distribution of the hidden variables prior to measurement given a set of chosen measurement settings and knowledge of the distribution of measurement outcomes. Such inferred distributions are naturally measurement dependent.

The plan for the paper is as follows. In section II we discuss the process of inference and how it differs from more familiar processes of probabilistic reasoning. In section III we demonstrate that the upper bound of the Clauser-Horne-Shimony-Holt (CHSH) parameter may be raised by relaxing measurement independence. We consider the usual system of two spin 1/2 particles prepared in the singlet state where each particle is subjected to measurement along one of two possible spin axes. The essential ideas are captured in a toy model described in Section IV. We consider measurement outcomes that break the CHSH bound and relate them dynamically to initial hidden variable conditions. In sections V and VI we illustrate analytically and numerically, respectively, how the CHSH bound may be raised significantly enough to account for the quantum correlations. How the upper bound evolves over time is also explored for a range of different dynamical models. Some models are able to yield a raised upper bound even when the time between system preparation and measurement is very long, whilst for other dynamical models the measurement dependence is destroyed over time. We explore the conditions for which measurement dependence emerges and persists long enough to account for quantum correlations.

## II. BACKWARDS IN TIME INFERENCE

Our reasoning runs backwards in time from information about measurement outcomes to making inferences about prior probability distributions. This is perhaps less familiar than relating future outcomes to earlier situations and a brief discussion is worth having in order not to confuse the approach with retrocausality.

We can imagine a similar process of inference in a different context. Consider two couples both of whom had a child some years ago. In the absence of further information, the likelihood assigned by an observer to various gender configurations in this situation would naturally be split equally between four possibilities: girl-girl, boy-boy, boy-girl, girl-boy. Since the couples are unknown to each other the observer would not expect the probability distribution over the gender of the child of one couple to have affected the probability of the gender of the child of the other. However, if the observer learns that the couples have a common biological grandchild, this affects the possible prior probability distributions. A correlation between the genders of the children emerges with equal likelihoods of girl-boy and boy-girl, and zero likelihood for the other two. Clearly the existence of a grandchild common to both couples could not have influenced the

probability distributions for the genders of their children assigned before their births. The influence we are considering is not retrocausal but rather a conditioning of past uncertainty given the availability of information about the present.

We apply a similar inference process to the Bell experiment of two entangled spin 1/2 particles, in the singlet state, undergoing measurements of spin components. If the outcomes of measurements are encoded in the hidden variables, we may infer the probability distribution of the hidden variables before measurement, given a set of chosen measurement settings, an associated distribution of measurement outcomes, and a model of the dynamics associated with measurement.

These inferred probability distributions do not correspond to the distributions from which the hidden variable configurations might have been sampled prior to measurement. Our concern is not with the selection of such initial configurations. Our reasoning works backward from measurement outcomes rather than forward from the selection of initial hidden variables. The distribution reveals to us the necessary configurations that the hidden variables would have had to adopt in order to generate the observed quantum correlations according to the dynamical model. Certain initial configurations of hidden variables before measurement may be more or less likely to have prevailed, depending on which measurement axis was chosen and potentially the measurement outcome. Some hidden variable configurations may even be inaccessible given a particular choice of measurement and the resulting outcome.

This reasoning shares commonality with the concept of quantum contextuality, where depending on the overall measurement context, only a subset of measurement outcomes that might have been thought possible are actually realisable [41–43]. Measurement dependence often is attributed to a correlation between the prepared initial state of the entangled particles and the measurement settings, such that the initial state somewhat determines which measurement settings may be chosen [10, 24, 30, 44]. We however do not think of measurement dependence in these terms, but rather that the inferred initial probability distribution of the hidden variables changes according to the chosen measurement setting, thus the hidden variables are contextual. The use of non-contextual hidden variables has previously been identified as a potential loophole of Bell’s theorem [45–47]. Since the possible measurement settings are non-commuting, it is natural that the probability distribution over the hidden variables should change with each measurement context [45–47]. Under this interpretation, measurement dependence can therefore be regarded as a form of contextuality.

### III. RELAXING THE UPPER BOUND OF THE CHSH PARAMETER

The CHSH parameter,  $S(\hat{a}, \hat{b}, \hat{a}', \hat{b}')$ , is defined as [48]

$$S = |C(\hat{a}, \hat{b}) - C(\hat{a}, \hat{b}')| + |C(\hat{a}', \hat{b}) + C(\hat{a}', \hat{b}')|, \quad (1)$$

where  $C(\hat{a}, \hat{b})$  is the correlation function of spin component measurement outcomes  $A$  and  $B$  (each taking values  $\pm 1$ ) for particle 1 undergoing a spin measurement along axis  $\hat{a}$  and particle 2 along axis  $\hat{b}$ , respectively. This may be written  $C(\hat{a}, \hat{b}) = \bar{AB} = P_{++}^{\hat{a}, \hat{b}} - P_{+-}^{\hat{a}, \hat{b}} - P_{-+}^{\hat{a}, \hat{b}} + P_{--}^{\hat{a}, \hat{b}}$ , where  $P_{\pm\pm}^{\hat{a}, \hat{b}}$  are the probabilities of measurement outcomes  $A = \pm 1, B = \pm 1$  along the respective axes. Each correlation function takes a value between  $\pm 1$  and  $S$  could therefore lie between 0 and 4.

Assuming that the outcome of measurement of particle 2 is not influenced by the choice of axis setting nor the outcome of measurement of particle 1, and vice versa, and also assuming that the system prior to measurement is specified by a set of hidden variables  $\lambda$  adopted according to a probability density function (pdf)  $\rho(\lambda)$ , then  $P_{\pm\pm}^{\hat{a}, \hat{b}} = \int p_{1\pm}^{\hat{a}}(\lambda) p_{2\pm}^{\hat{b}}(\lambda) \rho(\lambda) d\lambda$  where  $p_{1\pm}^{\hat{a}}(\lambda)$  are the probabilities of outcomes  $\pm 1$  for the spin component of particle 1 along axis  $\hat{a}$ , for a given specification of hidden variables, and with a similar meaning for  $p_{2\pm}^{\hat{b}}(\lambda)$ .

Measurement independence is the claim that the distribution of the hidden variables before measurement is not correlated with the chosen measurement settings: we use a pdf  $\rho(\lambda)$  rather than the conditioned pdf  $\rho(\lambda|\hat{n}_1, \hat{n}_2)$  where  $\hat{n}_1$  and  $\hat{n}_2$  denote axis orientations for measurements on particle 1 and particle 2 respectively.

Bell's analysis based on these assumptions requires  $S$  to have an upper bound of 2. The crucial observation is that

$$|\bar{B}(\hat{b}, \lambda) - \bar{B}(\hat{b}', \lambda)| + |\bar{B}(\hat{b}, \lambda) + \bar{B}(\hat{b}', \lambda)| \leq 2, \quad (2)$$

where  $\bar{B}(\hat{b}, \lambda) = p_{2+}^{\hat{b}}(\lambda) - p_{2-}^{\hat{b}}(\lambda)$  is the mean outcome of measurement of the spin component of particle 2 along axis  $\hat{b}$  for a given set of hidden variables  $\lambda$ . Note also that  $|\bar{B}(\hat{b}, \lambda)| \leq 1$  and that  $C(\hat{a}, \hat{b}) = \bar{AB} = \int \bar{A}(\hat{a}, \lambda) \bar{B}(\hat{b}, \lambda) \rho(\lambda) d\lambda$ . Since the mean outcome of spin component measurement for particle 1 along axis  $\hat{a}$  does not depend on the orientation of axis  $\hat{b}$  specifying the spin component measurement of particle 2, and vice versa, the average of  $AB$  given  $\hat{a}, \hat{b}$  and  $\lambda$  factorises, namely  $\bar{AB}(\hat{a}, \hat{b}, \lambda) = \bar{A}(\hat{a}, \lambda) \bar{B}(\hat{b}, \lambda)$ .

It has nevertheless been shown that the upper bound  $S \leq 2$  can be violated experimentally, requiring an examination of the assumptions made in the analysis. We seek to relax the assumption of measurement independence and demonstrate that this can raise the upper bound of the CHSH parameter.

The conceptual framework for this presumes that the process of measurement drives hidden system variables  $\lambda$

towards various measurement setting-dependent attractors in their phase space that correspond to spin component outcomes for those axis orientations. The chosen measurement axes and the rules of evolution allow us, in principle, to deduce the probability density over configurations of  $\lambda$  prior to measurement. Since the attractors depend on the measurement settings, the prior pdf  $\rho$  is therefore conditioned on the choice of axes, such that the correlation function should be written

$$C(\hat{a}, \hat{b}) = \int \bar{A}(\hat{a}, \lambda) \bar{B}(\hat{b}, \lambda) \rho(\lambda|\hat{a}, \hat{b}) d\lambda, \quad (3)$$

using notation to indicate the conditioning of  $\rho$ .

The CHSH parameter is built from correlation functions involving four pairs of measurement axes, and hence four conditioned pdfs over  $\lambda$ , which we denote  $\rho(\lambda|\hat{a}, \hat{b})$ ,  $\rho(\lambda|\hat{a}, \hat{b}')$ ,  $\rho(\lambda|\hat{a}', \hat{b})$  and  $\rho(\lambda|\hat{a}', \hat{b}')$ . We can use these to define a normalised average pdf  $\bar{\rho}(\lambda, \hat{a}, \hat{b}, \hat{a}', \hat{b}') = \frac{1}{4} (\rho(\lambda|\hat{a}, \hat{b}) + \rho(\lambda|\hat{a}, \hat{b}') + \rho(\lambda|\hat{a}', \hat{b}) + \rho(\lambda|\hat{a}', \hat{b}'))$  together with combinations that describe the differences between them:

$$\begin{aligned} \bar{\rho}\epsilon &= \frac{1}{4} (\rho(\lambda|\hat{a}, \hat{b}) - \rho(\lambda|\hat{a}, \hat{b}') + \rho(\lambda|\hat{a}', \hat{b}) - \rho(\lambda|\hat{a}', \hat{b}')) \\ \bar{\rho}\sigma &= \frac{1}{4} (\rho(\lambda|\hat{a}, \hat{b}) + \rho(\lambda|\hat{a}, \hat{b}') - \rho(\lambda|\hat{a}', \hat{b}) - \rho(\lambda|\hat{a}', \hat{b}')) \\ \bar{\rho}\eta &= \frac{1}{4} (\rho(\lambda|\hat{a}, \hat{b}) - \rho(\lambda|\hat{a}, \hat{b}') - \rho(\lambda|\hat{a}', \hat{b}) + \rho(\lambda|\hat{a}', \hat{b}')), \end{aligned} \quad (4)$$

such that  $\rho(\lambda|\hat{a}, \hat{b}) = \bar{\rho}(1 + \epsilon + \sigma + \eta)$ ,  $\rho(\lambda|\hat{a}, \hat{b}') = \bar{\rho}(1 - \epsilon + \sigma - \eta)$ ,  $\rho(\lambda|\hat{a}', \hat{b}) = \bar{\rho}(1 + \epsilon - \sigma - \eta)$ , and  $\rho(\lambda|\hat{a}', \hat{b}') = \bar{\rho}(1 - \epsilon - \sigma + \eta)$ . The  $\epsilon$ ,  $\sigma$  and  $\eta$  functions depend on all four axis orientations as well as  $\lambda$ .

Now consider the first combination of correlation functions in the CHSH parameter,  $C(\hat{a}, \hat{b}) - C(\hat{a}, \hat{b}')$ . Introducing conditioning of the probability densities according to the chosen measurement axes this can be written as

$$\begin{aligned} &\int \bar{A}(\hat{a}, \lambda) (\bar{B}(\hat{b}, \lambda) \rho(\lambda|\hat{a}, \hat{b}) - \bar{B}(\hat{b}', \lambda) \rho(\lambda|\hat{a}, \hat{b}')) d\lambda \\ &= \int \bar{A}(\hat{a}, \lambda) (\bar{B}(\hat{b}, \lambda) - \bar{B}(\hat{b}', \lambda)) \bar{\rho}(\lambda) d\lambda \\ &+ \int \bar{A}(\hat{a}, \lambda) (\bar{B}(\hat{b}, \lambda) + \bar{B}(\hat{b}', \lambda)) \bar{\rho}(\lambda) \epsilon(\lambda) d\lambda \\ &+ \int \bar{A}(\hat{a}, \lambda) (\bar{B}(\hat{b}, \lambda) - \bar{B}(\hat{b}', \lambda)) \bar{\rho}(\lambda) \sigma(\lambda) d\lambda \\ &+ \int \bar{A}(\hat{a}, \lambda) (\bar{B}(\hat{b}, \lambda) + \bar{B}(\hat{b}', \lambda)) \bar{\rho}(\lambda) \eta(\lambda) d\lambda, \end{aligned} \quad (5)$$

which, since  $|\bar{A}(\hat{a}, \lambda)| \leq 1$ , implies that

$$\begin{aligned} |C(\hat{a}, \hat{b}) - C(\hat{a}, \hat{b}')| &\leq \int |\bar{B}(\hat{b}, \lambda) - \bar{B}(\hat{b}', \lambda)| \bar{\rho}(\lambda) d\lambda \\ &+ \int |\bar{B}(\hat{b}, \lambda) + \bar{B}(\hat{b}', \lambda)| \bar{\rho}(\lambda) |\epsilon(\lambda)| d\lambda \\ &+ \int |\bar{B}(\hat{b}, \lambda) - \bar{B}(\hat{b}', \lambda)| \bar{\rho}(\lambda) |\sigma(\lambda)| d\lambda \\ &+ \int |\bar{B}(\hat{b}, \lambda) + \bar{B}(\hat{b}', \lambda)| \bar{\rho}(\lambda) |\eta(\lambda)| d\lambda. \end{aligned} \quad (6)$$

Similarly the combination  $C(\hat{a}', \hat{b}) + C(\hat{a}', \hat{b}')$  may be written

$$\begin{aligned} &\int \bar{A}(\hat{a}', \lambda) \left( \bar{B}(\hat{b}, \lambda) \rho(\lambda | \hat{a}', \hat{b}) + \bar{B}(\hat{b}', \lambda) \rho(\lambda | \hat{a}', \hat{b}') \right) d\lambda \\ &= \int \bar{A}(\hat{a}', \lambda) \left( \bar{B}(\hat{b}, \lambda) + \bar{B}(\hat{b}', \lambda) \right) \bar{\rho}(\lambda) d\lambda \\ &+ \int \bar{A}(\hat{a}', \lambda) \left( \bar{B}(\hat{b}, \lambda) - \bar{B}(\hat{b}', \lambda) \right) \bar{\rho}(\lambda) \epsilon(\lambda) d\lambda \\ &+ \int \bar{A}(\hat{a}', \lambda) \left( -\bar{B}(\hat{b}, \lambda) - \bar{B}(\hat{b}', \lambda) \right) \bar{\rho}(\lambda) \sigma(\lambda) d\lambda \\ &+ \int \bar{A}(\hat{a}', \lambda) \left( -\bar{B}(\hat{b}, \lambda) + \bar{B}(\hat{b}', \lambda) \right) \bar{\rho}(\lambda) \eta(\lambda) d\lambda, \end{aligned} \quad (7)$$

which, since  $|\bar{A}(\hat{a}, \lambda)| \leq 1$ , leads to

$$\begin{aligned} |C(\hat{a}', \hat{b}) + C(\hat{a}', \hat{b}')| &\leq \int |\bar{B}(\hat{b}, \lambda) + \bar{B}(\hat{b}', \lambda)| \bar{\rho}(\lambda) d\lambda \\ &+ \int |\bar{B}(\hat{b}, \lambda) - \bar{B}(\hat{b}', \lambda)| \bar{\rho}(\lambda) |\epsilon(\lambda)| d\lambda \\ &+ \int |\bar{B}(\hat{b}, \lambda) + \bar{B}(\hat{b}', \lambda)| \bar{\rho}(\lambda) |\sigma(\lambda)| d\lambda \\ &+ \int |\bar{B}(\hat{b}, \lambda) - \bar{B}(\hat{b}', \lambda)| \bar{\rho}(\lambda) |\eta(\lambda)| d\lambda. \end{aligned} \quad (8)$$

Combining Eqs. (6), (8) and (2), the CHSH parameter satisfies

$$S \leq 2 + \mu, \quad (9)$$

where

$$\mu = 2 \left( \int \bar{\rho}(|\epsilon| + |\sigma| + |\eta|) d\lambda \right) \geq 0 \quad (10)$$

represents an elevation of the usual upper limit. Note that  $\epsilon = \sigma = \eta = 0$  and hence  $\mu = 0$  in the absence of measurement dependence. Also, if only one of the four probability densities is non-zero for a given  $\lambda$ , an extreme case of measurement dependence, then  $\bar{\rho}|\epsilon|$ ,  $\bar{\rho}|\sigma|$  and  $\bar{\rho}|\eta|$  are all normalised to unity, in which case  $\mu = 6$ , though it should be noted that values of  $\mu$  above 2 are redundant since  $S$  cannot exceed 4.

#### IV. A TOY MODEL

We consider two hidden variables  $\lambda_1$  and  $\lambda_2$  that separately describe the state of each particle in a Bell exper-

iment. These variables evolve dynamically under measurement such that trajectories link the values associated with a measurement outcome to those describing the initial state of the system at time  $-t$ .

The post-measurement values of the hidden variables  $\lambda_1$  and  $\lambda_2$  are illustrated on the left hand side of Figure 1 as the large blue and orange circles, respectively, with the associated spin outcome indicated as black arrows. From these measurement results we work backwards using the hidden variable dynamics to infer possible initial values of  $\lambda_1$  and  $\lambda_2$ , illustrated as the blue and orange circles on the right and connected to their measurement outcomes by trajectories in the  $\lambda_1$  and  $\lambda_2$  phase spaces. We can hence compute the conditioned probability distributions  $\rho(\lambda_1, \lambda_2 | \hat{n}_1, \hat{n}_2)_t$  at the time  $-t$  when the system was prepared. From these we are able to calculate the corresponding additional term  $\mu(t)$  in the CHSH bound using Eq. (9). Our aim is to explore whether the dynamics allows sufficient measurement setting dependence of the initial probability distributions to raise the bound sufficiently to accommodate the asserted measurement results.

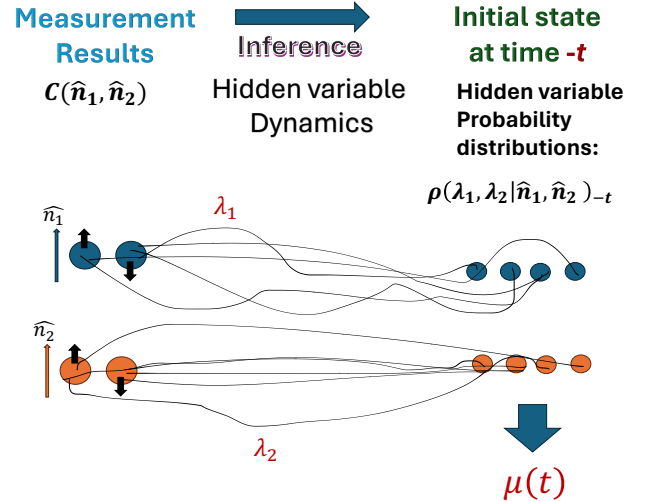


Figure 1. The strategy to find the additional term  $\mu$  in the upper bound on the CHSH parameter. We work backwards in time from measurement outcomes on the left to initial conditions on the right using a model of the hidden variable dynamics. If the measurement outcomes break the upper bound on the CHSH parameter, then the initial conditioned probability distributions for the hidden variables must possess sufficient measurement setting dependence to raise the bound appropriately. See text for details.

To illustrate this situation in a more concrete fashion, we consider two discrete hidden variables  $\lambda_1$  and  $\lambda_2$  and a phase space in the form of a grid of squares labelled with integer values.  $\lambda_1$  describes the state of the first particle in the entangled spin 1/2 particle pair and  $\lambda_2$  the second. The measurement of properties  $A$  and  $B$  of particle 1 and particle 2 respectively, is represented by attraction under the dynamics of each of  $\lambda_1$  and  $\lambda_2$  towards

one of two points, yielding four ‘targets’ at coordinates  $(\lambda_1^\pm, \lambda_2^\pm)$ . These represent the four possible combinations of spin measurement outcomes of the entangled particle pair: the situation is illustrated in Figure 2. The idea is that interactions between the system and measuring device bring about a dynamical evolution of the  $\lambda_1$  and  $\lambda_2$  to attractors (here fixed points) located at the targets. The outcome of the measurement of each property is  $\pm 1$ , as designated by the superscripts on the target coordinates.

We consider a situation where passage to each target arises from separate basins of attraction in the phase space [49]. These are shown in Figure 2(a) as four shades of grey: the measurement dynamics can generate trajectories starting from any of the black squares, for example, all of which terminate at the top right target  $(\lambda_1^+, \lambda_2^+)$ .

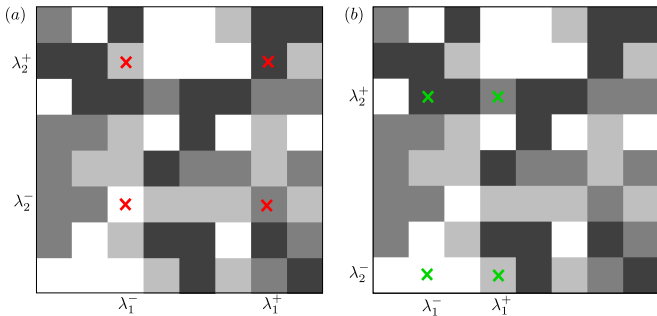


Figure 2. A discrete representation of the basins of attraction, over a phase space of configurations of hidden variables, associated with four measurement outcomes shown as crosses. All the initial configurations denoted by one of the four shades of grey evolve under measurement towards the appropriately shaded attractor coordinate pair  $(\lambda_1^\pm, \lambda_2^\pm)$  indicated by a cross  $\times$ . Situations (a) and (b) correspond to measurement of different system properties with distinct sets (indicated by colours) of attractors and associated basins.

The probabilities of adopting each black square prior to measurement would accumulate under the dynamics to generate a probability  $P_{++}$  of an outcome  $A = B = +1$  associated with arrival of the system at the  $(\lambda_1^+, \lambda_2^+)$  target, post-measurement. The suffixes in this probability correspond to the superscripts on the target coordinates. Conversely, if we wish to deduce the probabilities of having started out on a black square conditioned on information about which measurement is performed and its outcome, then we need to distribute the probability  $P_{++}$  of arrival at  $(\lambda_1^+, \lambda_2^+)$  after measurement over the basin of attraction of that target at earlier times, again in accordance with the measurement dynamics.

We can now see how such conditioned probabilities depend on the measurement concerned, represented in the toy model as attraction towards a different set of targets. Consider targets represented by the green crosses in Figure 2(b). The basins of attraction under the measurement dynamics might form a different pattern for these targets. There would be different probabilities of adop-

tion of configurations prior to measurement when conditioned on a measurement defined by the green crosses. This is compounded if we consider probabilities of arrival  $P_{\pm\pm}$  (probabilities associated with measurement outcomes) at the green and red targets that differ from one another.

It is crucial for the emergence of measurement dependence in this toy model that the phase space should be separated into basins of attraction to each outcome target for each measurement situation. We shall investigate cases where this is not the case later on and find that there is then insufficient measurement dependence in the initial probability distributions to accommodate the asserted measurement outcomes. In systems where the evolution is deterministic, outcomes are encoded in the coordinates describing the initial state and basins of attraction would be natural. For systems governed by stochastic dynamics such encoding could persist to some degree depending on the situation.

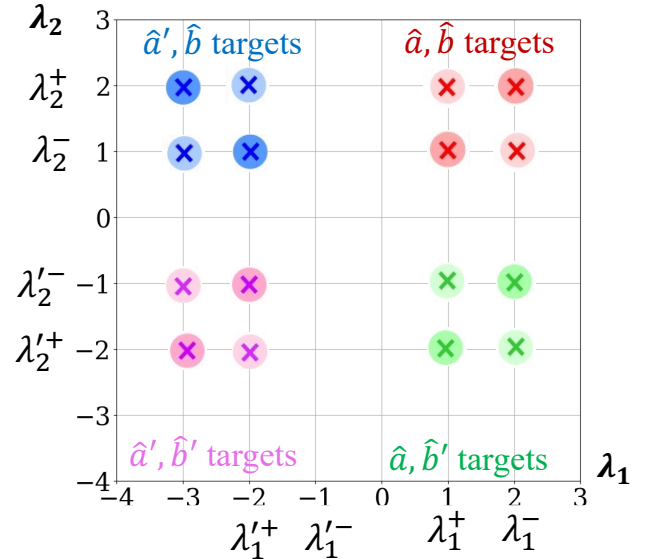


Figure 3. Configurations of the toy model are represented by grid squares in a two dimensional discrete phase space with integer coordinates  $\lambda_1$  and  $\lambda_2$ . The process of measurement draws the configuration towards one of four targets, shown as crosses in a specific colour, representing the four outcomes of measurement of properties  $A$  and  $B$ . Four different experimental circumstances are designated by labels  $\hat{a}, \hat{b}$ , etc, and distinguished by different colours. Arrival at one of the targets yields an outcome  $A = \pm 1$  and  $B = \pm 1$  according to the superscripts of the target coordinates. The probability of such an outcome is indicated by coloured circles at the targets: the darker the shade, the higher the probability  $P_{\pm\pm}^{x,y}$  of arrival at that target.

We now consider four possible measurement situations: settings  $\hat{a}, \hat{a}'$  with outcomes  $A$  concern particle 1, and  $\hat{b}, \hat{b}'$  with outcomes  $B$  concern particle 2. We illustrate the possible measurement setting combinations and their

associated distributions of measurement outcomes in Figure 3. We define four sets of targets for the measurement dynamics that evolve the variables  $\lambda_1$  and  $\lambda_2$ . The target pairs  $\lambda_1^\pm$  and  $\lambda_1'^\pm$  will be associated with ‘axis choices’  $\hat{a}$  and  $\hat{a}'$ , respectively, and  $\lambda_2^\pm$  and  $\lambda_2'^\pm$  are to be associated with ‘axes’  $\hat{b}$  and  $\hat{b}'$ . The terminology is chosen to establish an analogy with spin component measurement, and the superscripts indicate the outcome values  $\pm 1$  for properties  $A$  and  $B$ . The four measurement situations are specified by the choice of blue, red, pink or green targets in Figure 3. We associate  $+1$  outcomes with targets situated at even label positions on the grid and  $-1$  outcomes with odd labels.

We can then consider a set of probabilities  $P_{\pm\pm}^{\hat{x},\hat{y}}$  for post-measurement arrival of the system at each of the four targets in each group, for measurement settings  $\hat{x} = \hat{a}$  or  $\hat{a}'$  and  $\hat{y} = \hat{b}$  or  $\hat{b}'$ . These represent the probability distributions of measurement outcomes for a given pair of measurement settings. Figure 3 shows the targets as circular symbols with different shades of colour to indicate the magnitude of the probability of arrival at that target. To simplify the situation, we impose conditions  $P_{++}^{\hat{x},\hat{y}} = P_{--}^{\hat{x},\hat{y}}$  and  $P_{+-}^{\hat{x},\hat{y}} = P_{-+}^{\hat{x},\hat{y}}$ . Furthermore, we consider identical outcome probabilities for the red, blue and pink measurement situations, namely  $P_{\pm\pm}^{\hat{a},\hat{b}} = P_{\pm\pm}^{\hat{a}',\hat{b}} = P_{\pm\pm}^{\hat{a}',\hat{b}'}$ . However, we design the green measurement situation to be different by setting  $P_{\pm\mp}^{\hat{a},\hat{b}'} = P_{\pm\mp}^{\hat{a}',\hat{b}}$ , namely that dark and light shades of green characterise measurement outcomes coloured in light and dark shades, respectively, for the other three cases. This is to enable values of the CHSH parameter that exceed a value of two.

We can combine this description of measurement outcomes with a chosen pattern of basins of attraction associated with each target to derive the conditioned probabilities over the  $(\lambda_1, \lambda_2)$  phase space prior to measurement for each pair of chosen ‘axes’. Our aim is to produce a probability distribution  $P(\lambda_1, \lambda_2 | \hat{a}, \hat{b}')_{-t}$  over the phase space at time  $-t$  that is conditioned on outcomes at the green targets, and which differs from those conditioned on the blue, red and purple targets, which for simplicity we shall choose to be the same, namely  $P(\lambda_1, \lambda_2 | \hat{a}, \hat{b})_{-t} = P(\lambda_1, \lambda_2 | \hat{a}', \hat{b})_{-t} = P(\lambda_1, \lambda_2 | \hat{a}', \hat{b}')_{-t} \neq P(\lambda_1, \lambda_2 | \hat{a}, \hat{b}')_{-t}$ . The prior distribution over the hidden variables  $\lambda_1$  and  $\lambda_2$  then clearly depends on the measurement situation. Specifically, for the green measurement situation, there is a higher probability associated with the anti-correlated measurement outcomes, whereas correlated outcomes would be more probable in the other three measurement situations.

We then investigate whether the CHSH parameter implied by the toy model is compatible with a raised upper limit arising from the inferred measurement dependence and the additional term  $\mu$  in Eq. (9).

In order to represent the locality of measurement dynamics we require that the hidden variables should evolve independently of one another. The marginal distribution  $P(\lambda_1 | \hat{n}_1)_{-t} = \sum_{\lambda_2} P(\lambda_1, \lambda_2 | \hat{n}_1, \hat{n}_2)_{-t}$  is therefore inde-

pendent of the measurement axis chosen for the other particle (and similarly for  $P(\lambda_2 | \hat{n}_2)_{-t}$ ).

Finally, we reiterate that the ensembles of initial configurations of the system are inferred distributions of hidden variables conditioned on the measurement settings and dynamics presumed to operate. This should not be confused with a situation where nature somehow prepares the system with awareness of the yet to be made choice of the measurement settings. This is not what we are considering. The earlier discussion of the probability distributions of the genders of children borne to couples conditioned or not conditioned on whether they possess a common grandchild, illustrates this point. A grandchild does not influence the probabilities that governed the gender of its parents before their birth. The probability distributions in question simply represent the availability of relevant information at a later time.

We actually have no interest in probability distributions of hidden variables that are *not* conditioned on the measurement settings. It is the conditioned distributions that are relevant to the various measurement setting dependent correlation functions used in building the CHSH parameter.

## V. ASYMPTOTIC VALUE OF $\mu$ FOR SYMMETRIC RANDOM WALK DYNAMICS IN THE TOY MODEL

Let us first consider a measurement dynamics consisting of independent, symmetric random walks of the two hidden variables in two dimensions with equal probabilities of moving left or right with step-size  $|\Delta\lambda_1| = |\Delta\lambda_2| = 1$  per time-step, terminating at a target. The scheme means that working backwards for an even number of time-steps, the possible values of  $\lambda_1$  and  $\lambda_2$  (the basin of attraction) leading to a target with even values of  $\lambda_1$  and  $\lambda_2$  (an even-even target) also take even values, whereas for an odd number of time-steps  $\lambda_1$  and  $\lambda_2$  would both adopt odd values. Similarly, the possible values of  $\lambda_1$  and  $\lambda_2$  leading to an even-odd target will be even and odd respectively for an even number of time-steps and odd and even respectively for an odd number of time-steps. The even-oddness (parity) of possible values of  $\lambda_1$  and  $\lambda_2$  leading to a target therefore alternates with the time-step and from hereon we shall consider the situation at an even time-step. Thus we have a dynamics that defines certain basins of attraction for given outcomes on targets associated with specified measurement settings. For simplicity, we consider measurement to take place over a very large but even number of steps, namely  $t \rightarrow \infty$ . To this end we drop the suffix  $-t$  on the conditioned prior probability distribution over the phase space.

We also assume a phase space with an even number of locations in each dimension ( $N$  locations in all) and periodic boundary conditions. This means that the probability  $P(\lambda_{1,2} | \hat{a}, \hat{b})$  at any even-even location in the phase space, prior to measurement with settings  $\hat{a}, \hat{b}$ , is a con-

stant  $P_{ee}^{\hat{a}, \hat{b}}$  given by the probability of arrival  $P_{++}^{\hat{a}, \hat{b}}$  at red target  $(\lambda_1^+, \lambda_2^+)$  divided by the number of such locations,  $N/4$ , namely  $P_{ee}^{\hat{a}, \hat{b}} = 4P_{++}^{\hat{a}, \hat{b}}/N$ . Similarly, the conditioned probability  $P_{eo}^{\hat{a}, \hat{b}}$  at an even-odd location on the grid prior to measurement is the arrival probability  $P_{+-}^{\hat{a}, \hat{b}}$  at red target  $(\lambda_1^+, \lambda_2^-)$  divided equally between all even-odd locations in the grid, or  $P_{eo}^{\hat{a}, \hat{b}} = 4P_{+-}^{\hat{a}, \hat{b}}/N$ . The conditioned probability at an odd-even location is  $P_{oe}^{\hat{a}, \hat{b}} = 4P_{-+}^{\hat{a}, \hat{b}}/N$  and for odd-odd locations it is  $P_{oo}^{\hat{a}, \hat{b}} = 4P_{--}^{\hat{a}, \hat{b}}/N$ . The same arguments apply to measurement situation  $\hat{a}, \hat{b}'$  with arrival probabilities  $P_{\pm\pm}^{\hat{a}, \hat{b}'}$  at green targets, measurement situation  $\hat{a}', \hat{b}$  with arrival probabilities  $P_{\pm\pm}^{\hat{a}', \hat{b}}$  at blue targets, and measurement situation  $\hat{a}', \hat{b}'$  with arrival probabilities  $P_{\pm\pm}^{\hat{a}', \hat{b}'}$  at purple targets.

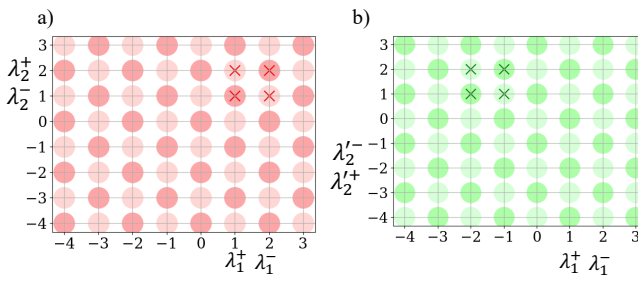


Figure 4. Probability distributions characterising the adoption of hidden variable configurations for a very large even number of timesteps prior to measurement of property  $AB$  in experimental circumstances (a)  $\hat{a}, \hat{b}$  and (b)  $\hat{a}', \hat{b}'$ , shown on the left and right in red and green, respectively, with the shades representing magnitude. These are conditioned on (i) the locations of the targets  $\lambda_1^\pm, \lambda_2^\pm$  in the grid to which the configurations are attracted by measurement dynamics consisting of independent symmetric random walks in  $\lambda_1$  and  $\lambda_2$  with a step length of 1, and (ii) on the overall probabilities of reaching each of the targets. These are asymptotic distributions of probability after taking an even number of backward time-steps. Notice that the two conditioned probability distributions differ, which is measurement dependence.

What this means is that the conditioned probabilities on the phase space are repeated versions of the patterns of probabilities of arrival at the targets after measurement. This is illustrated in Figure 4(a) for the  $\hat{a}, \hat{b}$  measurement situation. The dark and light shades of red represent the two probabilities  $P_{ee}^{\hat{a}, \hat{b}}$  and  $P_{eo}^{\hat{a}, \hat{b}}$ , respectively, recalling that we have imposed  $P_{ee}^{\hat{a}, \hat{b}} = P_{oo}^{\hat{a}, \hat{b}}$  and  $P_{eo}^{\hat{a}, \hat{b}} = P_{oe}^{\hat{a}, \hat{b}}$ . The distribution  $P(\lambda_1, \lambda_2 | \hat{a}, \hat{b})$  illustrated is the discrete analogue of the pdf  $\rho(\lambda | \hat{a}, \hat{b})$  considered for the situation with a continuum of hidden variable values. Under our assumptions, the conditioned initial probability distributions for measurement situations  $\hat{a}', \hat{b}$  and  $\hat{a}', \hat{b}'$  are identical to the distribution shown for  $\hat{a}, \hat{b}$  (but would be illustrated in blue and pink, respectively).

However, the conditioned probability distribution for the situation  $\hat{a}, \hat{b}'$  shown in Figure 4(b) is different. A light shade of green, representing  $P_{ee}^{\hat{a}, \hat{b}'} = P_{eo}^{\hat{a}, \hat{b}}$ , lies at a location where a dark shade of red, representing  $P_{ee}^{\hat{a}, \hat{b}}$ , is found in Figure 4(a), and vice versa.

The analogue of the additional term in Eq. (9) for the toy model is a sum of magnitudes of differences between the probability distribution shown in red in Figure 4(a) and its blue, pink and green counterparts, analogous to  $\rho(\lambda | \hat{a}, \hat{b})$ ,  $\rho(\lambda | \hat{a}', \hat{b})$ ,  $\rho(\lambda | \hat{a}', \hat{b}')$  and  $\rho(\lambda | \hat{a}, \hat{b}')$ , respectively. For the simplified case under consideration, the first three distributions are identical and the fourth is different. This implies, in the notation of a continuum phase space, that  $\bar{\rho}\epsilon = -\bar{\rho}\sigma = \bar{\rho}\eta = \frac{1}{4}(\rho(\lambda | \hat{a}, \hat{b}) - \rho(\lambda | \hat{a}, \hat{b}'))$  and hence the additional term in the Bell inequality for  $S$  in these circumstances is  $\mu = \frac{3}{2} \int |\rho(\lambda | \hat{a}, \hat{b}) - \rho(\lambda | \hat{a}, \hat{b}')| d\lambda$ .

For the discrete phase space the integral is replaced by a sum of moduli of the differences in probability at each position of the grid conditioned on the red and green measurement outcomes. For the situation we have constructed, these differences are  $P_{ee}^{\hat{a}, \hat{b}} - P_{ee}^{\hat{a}, \hat{b}'}$  at even-even and odd-odd points on the grid, and  $P_{eo}^{\hat{a}, \hat{b}} - P_{eo}^{\hat{a}, \hat{b}'}$  at even-odd and odd-even points, and these quantities are given by  $\pm (P_{ee}^{\hat{a}, \hat{b}} - P_{eo}^{\hat{a}, \hat{b}})$ , respectively. The sum of moduli of probability differences over the grid is therefore  $N |P_{ee}^{\hat{a}, \hat{b}} - P_{eo}^{\hat{a}, \hat{b}}| = 4 |P_{++}^{\hat{a}, \hat{b}} - P_{+-}^{\hat{a}, \hat{b}}|$  and the additional term for the toy model with the dynamics specified is  $\mu = 6 |P_{++}^{\hat{a}, \hat{b}} - P_{+-}^{\hat{a}, \hat{b}}|$ .

Similarly, all four correlation functions can be specified in terms of  $P_{++}^{\hat{a}, \hat{b}}$  and  $P_{+-}^{\hat{a}, \hat{b}}$ , specifically  $C(\hat{a}, \hat{b}) = C(\hat{a}', \hat{b}) = C(\hat{a}', \hat{b}') = -C(\hat{a}, \hat{b}') = 2(P_{++}^{\hat{a}, \hat{b}} - P_{+-}^{\hat{a}, \hat{b}})$ . Thus the CHSH parameter is  $S = 4|C(\hat{a}, \hat{b})|$  and the additional term is  $\mu = 3|C(\hat{a}, \hat{b})|$ . Bell's analysis therefore requires that

$$S = 4|C(\hat{a}, \hat{b})| \leq 2 + \mu = 2 + 3|C(\hat{a}, \hat{b})|, \quad (11)$$

which is clearly satisfied for the relevant range  $0 \leq |C(\hat{a}, \hat{b})| \leq 1$ . We conclude that measurement dependence created by the dynamics of the hidden variables during the measurement process has elevated the upper limit to accommodate any imposed value of the CHSH parameter. Furthermore, the conditioning of the hidden variables on the measurement settings is retained even at an asymptotic time limit, which is due to the existence of basins of attraction.

## VI. NUMERICAL REALISATIONS OF TOY MODEL DYNAMICS

We now calculate the value of the upper bound of the additional term numerically for different models of the measurement dynamics and for non-asymptotic measurement conditions. We consider probability distributions

over the hidden variables  $P(\lambda_1, \lambda_2 | \hat{n}_1, \hat{n}_2)_{-t}$  at a time  $-t$  relative to the measurement at  $t = 0$  for measurement settings  $\hat{n}_1$  and  $\hat{n}_2$  for the first and second particle, respectively, writing

$$\begin{aligned} P(\lambda_1, \lambda_2 | \hat{n}_1, \hat{n}_2)_{-t} = & P_{++}^{\hat{n}_1, \hat{n}_2} p(\lambda_1 | \lambda_1^+, \hat{n}_1)_{-t} p(\lambda_2 | \lambda_2^+, \hat{n}_2)_{-t} \\ & + P_{-+}^{\hat{n}_1, \hat{n}_2} p(\lambda_1 | \lambda_1^-, \hat{n}_1)_{-t} p(\lambda_2 | \lambda_2^+, \hat{n}_2)_{-t} \\ & + P_{+-}^{\hat{n}_1, \hat{n}_2} p(\lambda_1 | \lambda_1^+, \hat{n}_1)_{-t} p(\lambda_2 | \lambda_2^-, \hat{n}_2)_{-t} \\ & + P_{--}^{\hat{n}_1, \hat{n}_2} p(\lambda_1 | \lambda_1^-, \hat{n}_1)_{-t} p(\lambda_2 | \lambda_2^-, \hat{n}_2)_{-t}, \end{aligned} \quad (12)$$

where  $p(\lambda_i | \lambda_i^\pm, \hat{n}_i)_{-t}$  is the conditional probability distribution over  $\lambda_i$  at time  $-t$  generated by the backward dynamics of  $\lambda_i$  given that at  $t = 0$  the system resides at target value  $\lambda_i^\pm$  appropriate to setting  $\hat{n}_i$ . As before, the  $P_{\pm\pm}^{\hat{n}_1, \hat{n}_2}$  are the outcome probabilities for measurement settings  $\hat{n}_1$  and  $\hat{n}_2$ , as illustrated in Figure 3.

We impose periodic boundaries on the values of  $(\lambda_1, \lambda_2)$  in such a way that they maintain their parity: even-even values outside the boundary get mapped to even-even values within the boundary and similarly for odd-odd, even-odd and odd-even coordinates. We set the size of the  $(\lambda_1, \lambda_2)$  phase space to be  $8 \times 8$ , with  $\lambda_{1,2}$  taking values between  $-4$  and  $+3$ . This can be achieved using  $\lambda_{PB} = ((\lambda + 4) \oplus 8) - 4$  where  $\lambda_{PB}$  is the value of  $\lambda$  after mapping through the periodic boundaries and  $\oplus$  represents a modulo function.

We present three models of measurement in the toy model that illustrate some of the issues. Further cases are studied in Appendices A and B.

### A. Symmetric random walk for finite time

We first calculate the probability distributions  $p(\lambda_1 | \lambda_1^\pm, \hat{n}_1)_{-t}$  and  $p(\lambda_2 | \lambda_2^\pm, \hat{n}_2)_{-t}$  for symmetric random walks with step size  $|\Delta\lambda| = 1$  per time-step, namely the model considered in section V but now for finite time. The probability of adopting a certain value of  $\lambda_i$  at a time  $-t$  corresponding to an even number of backward time-steps, given that the system reaches a target  $\lambda_i^\pm$  at  $t = 0$  for a chosen measurement axis  $\hat{n}$ , is then

$$p(\lambda_i | \lambda_i^\pm, \hat{n})_{-t} = \frac{1}{2^t} \frac{t!}{\left(\frac{t-\lambda_i+\lambda_i^\pm}{2}\right)! \left(\frac{t+\lambda_i-\lambda_i^\pm}{2}\right)!} \quad (13)$$

The possible starting points are then  $\lambda_i^\pm - t, \lambda_i^\pm - t + 2, \lambda_i^\pm - t + 4, \dots, \lambda_i^\pm + t - 4, \lambda_i^\pm + t - 2, \lambda_i^\pm - t$ . The probability distribution over both  $\lambda_1$  and  $\lambda_2$  can then be found through Eq. (12) using the probabilities of arrival given in Figure 3 and considering each of the possible targets (measurement outcomes) for a given measurement situation.

We calculate the additional term  $\mu$  in the Bell limit arising from the measurement dependence in the probability distributions  $P(\lambda_1, \lambda_2 | \hat{n}_1, \hat{n}_2)_{-t}$  given by Eq. (4).

Figure 5 shows that the additional term decreases to a value of around  $\approx 2.4$ , where it remains, even at  $t = 100$ , revealing that the conditioning of the probabilities of adopting hidden variables prior to measurement is persistent for this dynamical model, as was expected from the analytical calculations in section V.

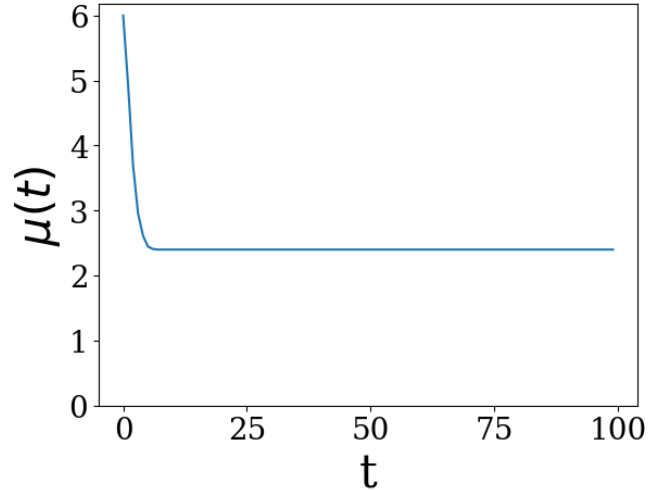


Figure 5. The numerically calculated additional term  $\mu(t)$  against time  $t$  running backwards from the moment of measurement at  $t = 0$ . The dynamics consist of independent symmetric random walks in  $\lambda_1$  and  $\lambda_2$  with a step size of unity. We use post-measurement outcome probabilities  $P_{\pm\pm}^{\hat{a}, \hat{b}} = P_{\pm\pm}^{\hat{a}', \hat{b}} = P_{\pm\pm}^{\hat{a}', \hat{b}'} = P_{\pm\mp}^{\hat{a}, \hat{b}'} = 0.45$  and  $P_{\pm\mp}^{\hat{a}, \hat{b}} = P_{\pm\mp}^{\hat{a}', \hat{b}} = P_{\pm\mp}^{\hat{a}', \hat{b}'} = 0.05$ .

Figure 6 A) depicts the probability distributions of  $\lambda_1$  and  $\lambda_2$  at  $t = 10$  for a)  $P(\lambda_1, \lambda_2 | \hat{a}, \hat{b})_{-t}$  and b)  $P(\lambda_1, \lambda_2 | \hat{a}, \hat{b}')_{-t}$ . A similar distribution to a) emerges for  $P(\lambda_1, \lambda_2 | \hat{a}', \hat{b})_{-t}$  and  $P(\lambda_1, \lambda_2 | \hat{a}', \hat{b}')_{-t}$ . It can be seen that at an even time-step, the higher probabilities in pattern a) lie at even-even and odd-odd points whilst for b) they lie at even-odd and odd-even points, a clear difference between  $P(\lambda_1, \lambda_2 | \hat{a}, \hat{b})_{-t}$  and the other three probability distributions. This results in a sufficiently high additional term to account for the imposed outcome correlations. Figure 6 (B) illustrates the possible values of  $\lambda_1$  and  $\lambda_2$  that lead to each target for settings  $\hat{a}, \hat{b}$  at  $t = 10$ . A similar plot is formed for the other settings pairs. Each target is associated with a unique set of possible prior values of  $\lambda_1$  and  $\lambda_2$ . Only even-even values of  $\lambda_1$  and  $\lambda_2$  lead to the even-even targets (at an even time-step) and similarly for other parities of the targets and  $\lambda_1$  and  $\lambda_2$ . There are therefore unique basins of attraction leading to each target for a given measurement situation.

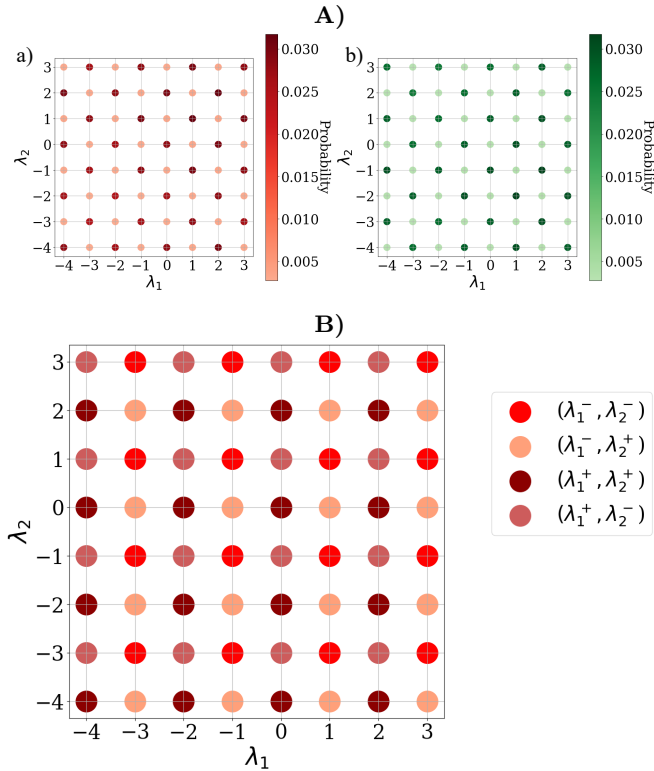


Figure 6. **A)** Probability distributions of the hidden variables  $\lambda_{1,2}$  for the different measurement settings: a)  $P(\lambda_1, \lambda_2 | \hat{a}, \hat{b})_{-t}$ , b)  $P(\lambda_1, \lambda_2 | \hat{a}, \hat{b}')_{-t}$ . Probabilities of arrival are  $P_{\pm\pm}^{\hat{a}, \hat{b}} = P_{\pm\pm}^{\hat{a}', \hat{b}'} = P_{\pm\mp}^{\hat{a}, \hat{b}'} = P_{\pm\mp}^{\hat{a}', \hat{b}} = 0.45$  and  $P_{\pm\mp}^{\hat{a}, \hat{b}} = P_{\pm\mp}^{\hat{a}', \hat{b}'} = P_{\pm\mp}^{\hat{a}', \hat{b}'} = P_{\pm\mp}^{\hat{a}, \hat{b}} = 0.05$ , calculated at  $t = 10$ . **B)** Possible values of  $\lambda_{1,2}$  leading to each of the four different targets  $(\lambda_1^\pm, \lambda_2^\pm)$  for the measurement setting pair  $(\hat{a}, \hat{b})$ .

Figure 7 depicts how the numerically calculated upper bound of the CHSH parameter (Eq. (1) (green) depends on the value of the correlation function  $C(\hat{a}, \hat{b})$  for the specified dynamics. The asymptotic value of the upper bound  $2 + \mu_{asym}$  (orange dots) is plotted alongside the numerically calculated value  $2 + \mu_{num}$  (blue dashes), found at time  $t = 10$ . Once again,  $t$  denotes how much time has elapsed between system preparation and measurement.

It can be seen in Figure 7 that the additional term can accommodate the corresponding value of the CHSH parameter. The asymptotic value of the additional term closely resembles the numerically calculated value. Naturally, the asymptotic and numerical values of the additional term become more similar as  $t$  increases.

Note that the additional term is nonzero asymptotically only when the size of the grid is even. When it is odd, the additional term vanishes as  $t \rightarrow \infty$  since the parity of the hidden variable is not maintained with time and the basins of attraction to each target mix. We consider another case of the elimination of the additional term in the next subsection.

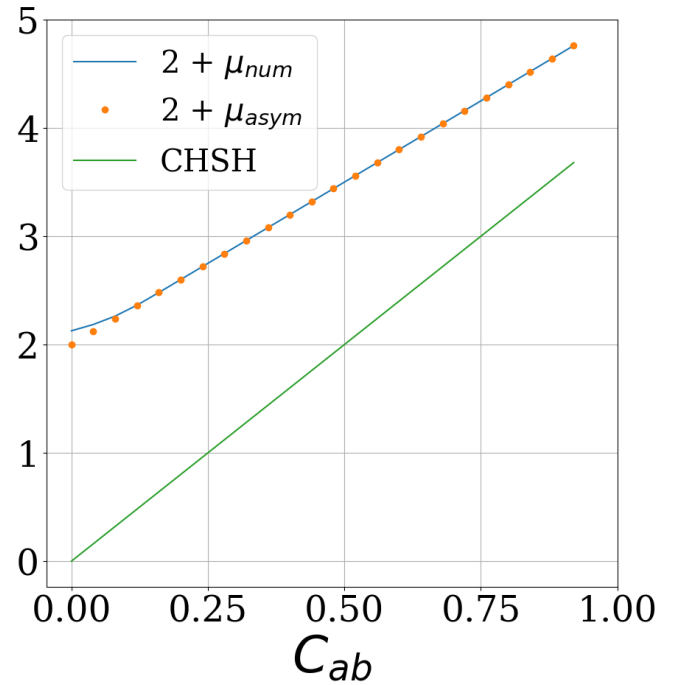


Figure 7. The upper bound  $2 + \mu$  of the CHSH parameter for different values of the correlation function  $C(\hat{a}, \hat{b})$  for a symmetric random walk on the phase space grid with point targets and equal probabilities of moving one space left or right.  $2 + \mu_{num}$  is calculated numerically at  $t = 10$  (blue curve) and compared with the asymptotic value of  $2 + \mu_{asym}$  (orange dots) and the corresponding value of the CHSH parameter (green). The post-measurement outcome probabilities form the same pattern as depicted in Figure 3, those with darker shades mean  $P_{\pm\pm}^{\hat{a}, \hat{b}} = P_{\pm\pm}^{\hat{a}', \hat{b}'} = P_{\pm\mp}^{\hat{a}, \hat{b}'} = P_{\pm\mp}^{\hat{a}', \hat{b}} = 0.48$  whilst those with the lighter shades correspond to  $P_{\pm\mp}^{\hat{a}, \hat{b}} = P_{\pm\mp}^{\hat{a}', \hat{b}'} = P_{\pm\mp}^{\hat{a}', \hat{b}'} = P_{\pm\mp}^{\hat{a}, \hat{b}} = 0.02$  varying from 0.02 to 0.48.

## B. Remaining still erases the additional term

We now consider dynamics with equal probabilities of moving left or right with step size 1 or of remaining still. The probability of adopting the initial hidden variable value  $\lambda_i$  at backward time-step  $t$ , given its arrival at a target  $\lambda_i^\pm$  for the measurement setting  $\hat{n}_i$  at  $t = 0$ , can be calculated using the following expression

$$p(\lambda_i | \lambda_i^\pm, \hat{n}_i)_{-t} = \sum_{N_r, N_l, N_s} \frac{1}{3^t} \frac{t!}{N_r! N_l! N_s!} \quad (14)$$

subject to the condition  $N_r + N_l + N_s = t$ .  $\lambda_i^\pm$  denotes the target (measurement outcome) for a given measurement setting  $\hat{n}_i$ ,  $N_r$  denotes the number of moves made to the right,  $N_l$  the number of moves made to the left, and  $N_s$  the number of times the hidden variable remains the same. The possible initial values of  $\lambda_i$  would then be given by  $\lambda_i = \lambda_i^\pm + N_r - N_l$ . The expression reflects that

there may be multiple combinations of values of  $N_r$ ,  $N_l$  and  $N_s$  that lead to the same value of  $\lambda_i$  and thus to yield the total probability of adopting a specific value of  $\lambda_i$ , we must add the probabilities of these contributions together.

We can use Eq. (14) to compute the probability distributions  $p(\lambda_1|\lambda_1^\pm, \hat{n}_1)_{-t}$  and  $p(\lambda_2|\lambda_2^\pm, \hat{n}_2)_{-t}$  and Eq. (12) provides the pdf  $P(\lambda_1, \lambda_2|\hat{n}_1, \hat{n}_2)_{-t}$ . We can then calculate how the additional term  $\mu$  varies with time using Eq. (4), shown in Figure 8 for a specific set of post-measurement outcome probabilities  $P_{\pm\pm}^{\hat{a}, \hat{b}}$  etc. It can be seen that it converges towards zero. Therefore these dynamics could not have been used to account for the asserted variation in correlation functions and CHSH parameter, the reason for which is the failure to maintain separate basins of attraction.

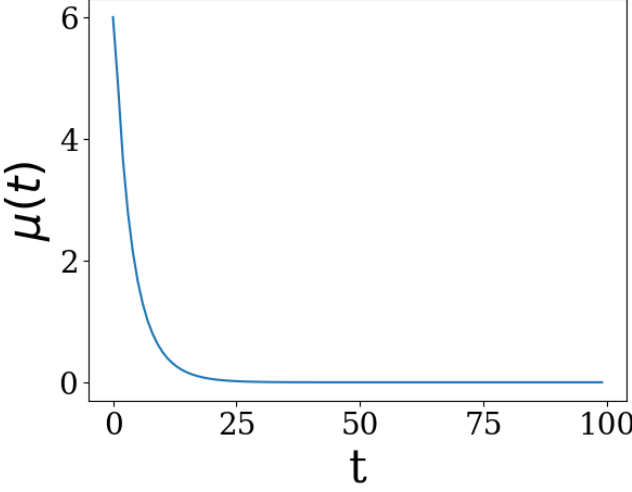


Figure 8. The variation of the additional term  $\mu$  with  $t$  for a symmetric random walk with equal probabilities of moving left or right or remaining still. Targets are as depicted in Figure 3.  $t$  denotes how much time has elapsed between system preparation and measurement. The post-measurement outcome probabilities are  $P_{\pm\pm}^{\hat{a}, \hat{b}} = P_{\pm\pm}^{\hat{a}', \hat{b}'} = P_{\pm\pm}^{\hat{a}'', \hat{b}''} = P_{\pm\mp}^{\hat{a}, \hat{b}'} = 0.45$  and  $P_{\pm\mp}^{\hat{a}, \hat{b}'} = P_{\pm\mp}^{\hat{a}', \hat{b}'} = P_{\pm\mp}^{\hat{a}'', \hat{b}''} = P_{\pm\pm}^{\hat{a}, \hat{b}'} = 0.05$ .

Figure 9 (A) depicts the probability distributions of the hidden variables at  $t = 10$  for (a)  $P(\lambda_1, \lambda_2|\hat{a}, \hat{b})_{-t}$  and (b)  $P(\lambda_1, \lambda_2|\hat{a}, \hat{b}')_{-t}$ . Unlike the symmetric random walk with equal probabilities of moving left and right, adding an option of remaining generates probability distributions with similar patterns for the different settings.

Figure 9 (B) shows possible values of  $\lambda_1$  and  $\lambda_2$  associated with each target for the measurement setting pair  $(\hat{a}, \hat{b})$ . Similar plots are formed for the other three measurement settings. All targets appear to be accessible from all possible values of  $\lambda_1$  and  $\lambda_2$ . There are therefore no unique basins of attraction and therefore very little difference between the hidden variable distributions in Figure 9 (A). Consequently there is no measurement

dependence the additional term in Figure 8 goes asymptotically to zero.

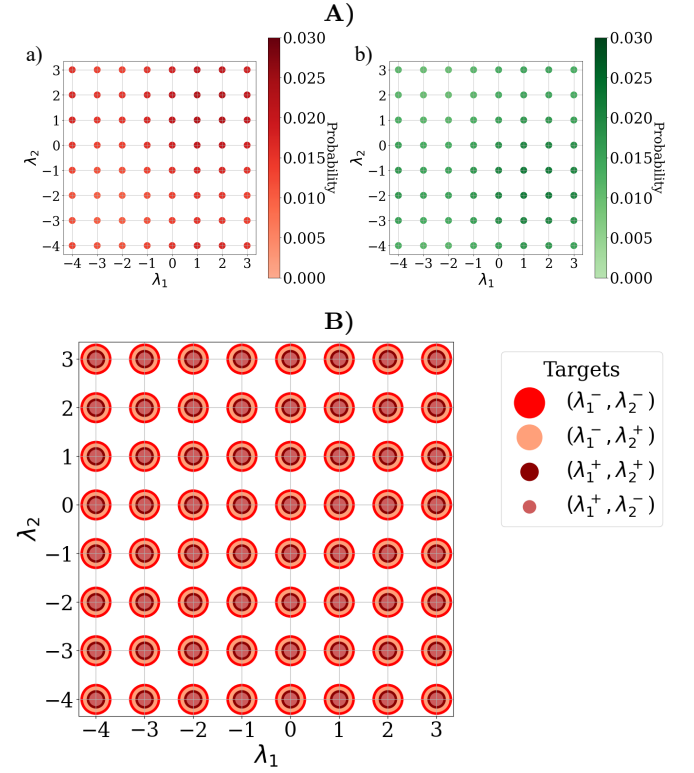


Figure 9. **A)** Probability distributions of the hidden variables at  $t = 10$  a)  $P(\lambda_1, \lambda_2|\hat{a}, \hat{b})_{-t}$  and b)  $P(\lambda_1, \lambda_2|\hat{a}, \hat{b}')_{-t}$  for a random walk with equal probabilities of remaining still or moving left or right by one spacing. The post-measurement outcome probabilities are  $P_{\pm\pm}^{\hat{a}, \hat{b}} = P_{\pm\pm}^{\hat{a}', \hat{b}'} = P_{\pm\pm}^{\hat{a}'', \hat{b}''} = P_{\pm\mp}^{\hat{a}, \hat{b}'} = 0.45$  and  $P_{\pm\mp}^{\hat{a}, \hat{b}'} = P_{\pm\mp}^{\hat{a}', \hat{b}'} = P_{\pm\mp}^{\hat{a}'', \hat{b}''} = P_{\pm\pm}^{\hat{a}, \hat{b}'} = 0.05$ . **B)** The possible values of  $\lambda_1$  and  $\lambda_2$  that lead to each of the four different targets  $(\lambda_1^\pm, \lambda_2^\pm)$  for setting  $(\hat{a}, \hat{b})$ .

### C. Broad targets

So far we have considered the targets (arrival at which signifies measurement outcomes) to be single points in the phase space of the hidden variables, characterised by their parity. Now we consider them to correspond to a collection of points that includes values of  $\lambda_1$  and  $\lambda_2$  of all parities. Figure 10 illustrates how each target is now broadened to comprise four points: an even-even, odd-odd, even-odd and an odd-even point. The post-measurement outcome probabilities for each target are divided equally between the four points. Measurement setting  $(\hat{a}, \hat{b})$  now has a  $A = -1$ ,  $B = -1$  target  $(\lambda_1^-, \lambda_2^-)$  comprised of the following four points  $(\lambda_1, \lambda_2) = (1, 1), (1, 2), (2, 2), (2, 1)$ , a  $(\lambda_1^+, \lambda_2^+)$  target comprised of  $(4, 4), (4, 5), (5, 5), (5, 4)$ , a  $(\lambda_1^+, \lambda_2^-)$  target made up of  $(4, 1), (4, 2), (5, 2), (5, 1)$  and a  $(\lambda_1^-, \lambda_2^+)$  target that includes  $(1, 4), (1, 5), (2, 4), (2, 5)$ , with a similar

pattern for the other three measurement axis pairs in their respective quadrants. The initial probability distributions over the values of  $\lambda_1$  and  $\lambda_2$  will be conditioned on later arrival at any of the four points within each target. We calculate the probability distributions  $P(\lambda_1, \lambda_2 | \hat{n}_1, \hat{n}_2)_{-t}$  and hence the additional term  $\mu$  using Eq. (4). We use the periodic boundaries of size 12 defined by  $\lambda = ((\lambda + 6) \oplus 12) - 6$ .

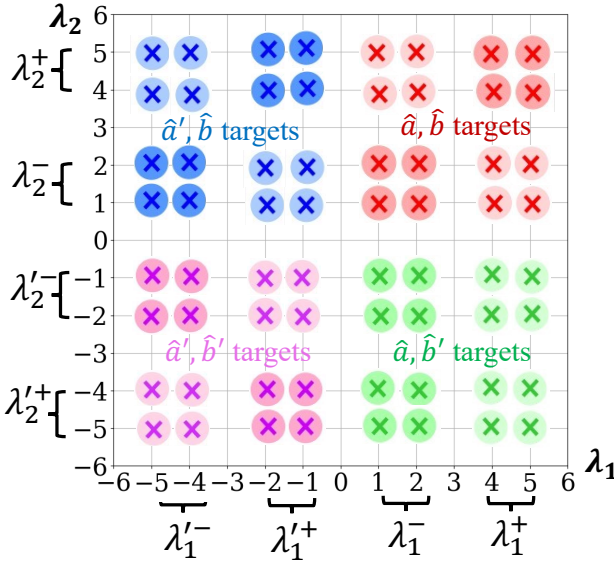


Figure 10. Broad targets (measurement outcomes) comprised of four points are used for each measurement setting. The darker the shade, the higher the post-measurement outcome probability. As before,  $P_{\pm\pm}^{\hat{a},\hat{b}} = P_{\pm\pm}^{\hat{a}',\hat{b}'} = P_{\pm\pm}^{\hat{a}',\hat{b}'} = P_{\pm\mp}^{\hat{a},\hat{b}'} = 0.45$  and  $P_{\pm\mp}^{\hat{a},\hat{b}} = P_{\pm\mp}^{\hat{a}',\hat{b}'} = P_{\pm\mp}^{\hat{a}',\hat{b}'} = P_{\pm\mp}^{\hat{a},\hat{b}'} = 0.05$ , with probability distributed evenly across the four points forming each target.

Figure 11 illustrates how the additional term evolves over time  $t$  running backwards from system measurement to preparation for a symmetric random walk with equal probabilities of moving left or right by one spacing and broad targets. The additional term decreases asymptotically towards zero indicating that such dynamics and targets are incompatible with assumed outcome probabilities that break the standard Bell bound.

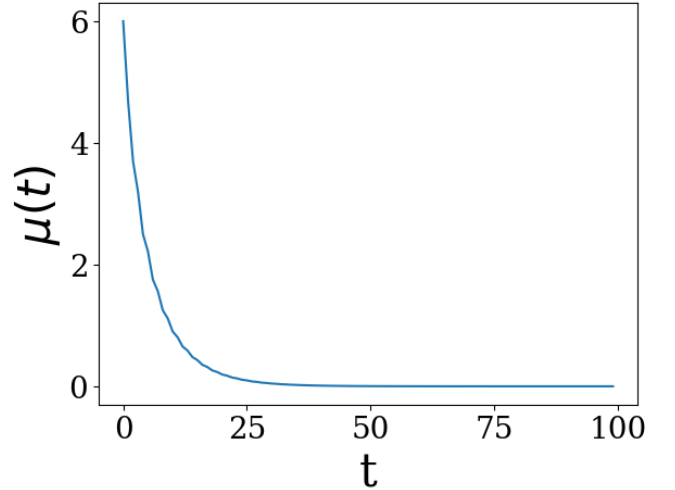


Figure 11. The variation of the additional term  $\mu$  with  $t$  for a symmetric random walk with equal probability of moving left or right by one spacing and broad targets which are as depicted in Figure 10. The outcome probabilities are  $P_{\pm\pm}^{\hat{a},\hat{b}} = P_{\pm\pm}^{\hat{a}',\hat{b}'} = P_{\pm\pm}^{\hat{a}',\hat{b}'} = P_{\pm\mp}^{\hat{a},\hat{b}'} = 0.45$  and  $P_{\pm\mp}^{\hat{a},\hat{b}} = P_{\pm\mp}^{\hat{a}',\hat{b}'} = P_{\pm\mp}^{\hat{a}',\hat{b}'} = P_{\pm\mp}^{\hat{a},\hat{b}'} = 0.05$ .

Figure 12 depicts the probability distributions over  $\lambda_1$  and  $\lambda_2$  for (a) measurement setting  $(\hat{a}, \hat{b})$  and (b)  $(\hat{a}, \hat{b}')$  at  $t = 10$ . As in Figure 9 (A), there are no significant differences between the probability distributions for the different measurement settings. There are no unique basins of attraction to each target and the additional term vanishes asymptotically. Measurement dependence is absent.

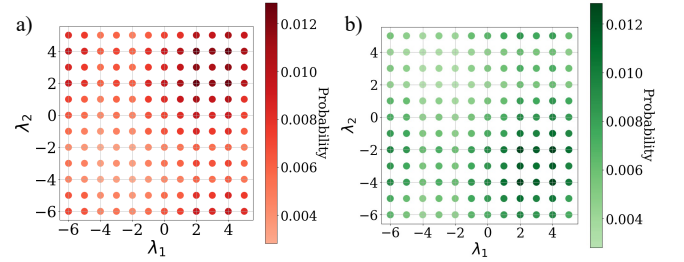


Figure 12. The probability distributions of the hidden variables  $\lambda_1$  and  $\lambda_2$  at  $t = 10$ : (a)  $P(\lambda_1, \lambda_2 | \hat{a}, \hat{b})_{-t}$  and (b)  $P(\lambda_1, \lambda_2 | \hat{a}, \hat{b}')_{-t}$  for a symmetric random walk with equal probability of moving left or right by one spacing and broad targets. The outcome probabilities are  $P_{\pm\pm}^{\hat{a},\hat{b}} = P_{\pm\pm}^{\hat{a}',\hat{b}'} = P_{\pm\pm}^{\hat{a}',\hat{b}'} = P_{\pm\mp}^{\hat{a},\hat{b}'} = 0.45$  and  $P_{\pm\mp}^{\hat{a},\hat{b}} = P_{\pm\mp}^{\hat{a}',\hat{b}'} = P_{\pm\mp}^{\hat{a}',\hat{b}'} = P_{\pm\mp}^{\hat{a},\hat{b}'} = 0.05$ .

## VII. CONCLUSIONS

Bell's inequalities rely on an assumption that the probability density  $\rho$  of hidden variables  $\lambda$  prior to measurement does not depend on the measurement settings chosen, a condition known as measurement independence.

If in a Bell experiment particle 1 undergoes a measurement of its spin along either axis  $\hat{a}$  or  $\hat{a}'$  and particle 2 undergoes a spin measurement along axis  $\hat{b}$  or  $\hat{b}'$ , then measurement independence is expressed by  $\rho(\lambda|\hat{a}, \hat{b}) = \rho(\lambda|\hat{a}', \hat{b}) = \rho(\lambda|\hat{a}, \hat{b}') = \rho(\lambda|\hat{a}', \hat{b}')$ . In this work we relax this assumption by imagining that measurement is a dynamic process involving attraction of the system towards fixed points in the hidden variable phase space that represent measurement outcomes. A suitable measurement dynamics together with fixed points that are specific to measurement settings can then lead to measurement dependence. We demonstrate that the upper bound of the CHSH parameter may be raised by an additional term  $\mu$ , defined by the sums and differences between the four hidden variable probability densities conditioned on the measurement settings. This can be large enough to accommodate measurement correlations that break the standard Bell bound.

The conditioned probability distributions of the hidden variables  $\rho(\lambda|\hat{n}_1, \hat{n}_2)$  need not correspond to a distribution from which the hidden variables might be selected to represent a prepared but uncertain entangled state. Rather, they demonstrate what the hidden variable statistics before measurement would have had to have been in order to account for the Bell bound breaking measurement correlations. Our reasoning works backward from measurement outcomes rather than forward from the selection of initial hidden variables. If the outcomes of measurements are encoded in the hidden variables, we may infer the probability density of the hidden variables before measurement, given a set of measurement settings, an associated distribution of measurement outcomes, and a model of the dynamics associated with measurement.

We consider a toy model where the dynamics of the hidden variables take the form of a symmetric random walk on a discrete space with periodic boundaries, and with equal probabilities of moving left or right. Variations in the dynamics are also explored. Measurement

drives the hidden variables towards post-measurement attractors (targets) defining measurement outcomes for the given measurement settings. We are able to infer the probability distributions of the hidden variables before measurement, given the chosen measurement settings and explore how the additional term  $\mu$  evolves with the amount of time between state preparation and measurement. Variations in the dynamics are explored to reveal key features required for measurement dependence to be significant.

The additional term depends on three features: the dynamics of the random walk, the size of the periodic boundaries and the level of coarse graining of the measurement outcomes (targets). The dynamics that successfully reproduce Bell bound breaking correlations are therefore delicate. What is required is that each target for a given measurement situation has to some extent a basin of attraction under the dynamics. We show this by introducing an additional probability of remaining still (as well as moving left or right) into the random walk dynamics, as well as coarse graining the targets such that they comprised multiple points on the phase space, which disturb the basins of attraction offered by the simple random walk.

Not unlike contextuality, we learn that in order to break the Bell bound it is necessary that only a subset of the possible values of the hidden variables should be capable of providing certain measurement outcomes for a specified measurement scenario.

## ACKNOWLEDGEMENTS

SMW is supported by a PhD studentship funded by Engineering and Physical Sciences Research Council (EPSRC) under grant codes EP/R513143/1 and EP/T517793/1.

---

[1] J. S. Bell, On the Einstein-Podolsky-Rosen paradox, *Physics* **1**, 195 (1964).

[2] A. Aspect, J. Dalibard, and G. Roger, Experimental Test of Bell's Inequalities Using Time-Varying Analyzers, *Physical Review Letters* **49**, 1804 (1982).

[3] M. Giustina, M. A. M. Versteegh, S. Wengerowsky, J. Handsteiner, A. Hochrainer, K. Phelan, F. Steinlechner, J. Kofler, J.-Å. Larsson, C. Abellán, W. Amaya, V. Pruneri, M. W. Mitchell, J. Beyer, T. Gerrits, A. E. Lita, L. K. Shalm, S. W. Nam, T. Scheidl, R. Ursin, B. Wittmann, and A. Zeilinger, Significant-Loophole-Free Test of Bell's Theorem with Entangled Photons, *Physical Review Letters* **115**, 250401 (2015).

[4] B. G. Christensen, K. T. McCusker, J. B. Altepeter, B. Calkins, T. Gerrits, A. E. Lita, A. Miller, L. K. Shalm, Y. Zhang, S. W. Nam, N. Brunner, C. C. W. Lim, N. Gisin, and P. G. Kwiat, Detection-Loophole-Free Test of Quantum Nonlocality, and Applications, *Physical Review Letters* **111**, 130406 (2013).

[5] B. Hensen, H. Bernien, A. E. Dréau, A. Reiserer, N. Kalb, M. S. Blok, J. Ruitenberg, R. F. L. Vermeulen, R. N. Schouten, C. Abellán, W. Amaya, V. Pruneri, M. W. Mitchell, M. Markham, D. J. Twitchen, D. Elkouss, S. Wehner, T. H. Taminiau, and R. Hanson, Loophole-free Bell inequality violation using electron spins separated by 1.3 kilometres, *Nature* **526**, 682 (2015).

[6] L. K. Shalm, E. Meyer-Scott, B. G. Christensen, P. Bierhorst, M. A. Wayne, M. J. Stevens, T. Gerrits, S. Glancy, D. R. Hamel, M. S. Allman, K. J. Coakley, S. D. Dyer, C. Hodge, A. E. Lita, V. B. Verma, C. Lambrocco, E. Tortorici, A. L. Migdall, Y. Zhang, D. R. Kumor, W. H. Farr, F. Marsili, M. D. Shaw, J. A. Stern, C. Abellán, W. Amaya, V. Pruneri, T. Jennewein, M. W. Mitchell, P. G. Kwiat, J. C. Bienfang, R. P. Mirin,

E. Knill, and S. W. Nam, Strong Loophole-Free Test of Local Realism, *Physical Review Letters* **115**, 250402 (2015).

[7] M. A. Rowe, D. Kielpinski, V. Meyer, C. A. Sackett, W. M. Itano, C. Monroe, and D. J. Wineland, Experimental violation of a Bell's inequality with efficient detection, *Nature* **409**, 791 (2001).

[8] J. S. Bell, *Speakable and Unspeakable in Quantum Mechanics: Collected Papers on Quantum Philosophy*, 2nd ed. (Cambridge University Press, Cambridge, 2004).

[9] T. Norsen, *Foundations of Quantum Mechanics: An Exploration of the Physical Meaning of Quantum Theory* (Springer, Cham, Switzerland, 2017).

[10] S. Hossenfelder and T. Palmer, Rethinking Superdeterminism, *Frontiers in Physics* **8** (2020).

[11] A. Sadhu and S. Das, Testing of quantum nonlocal correlations under constrained free will and imperfect detectors, *Physical Review A* **107**, 012212 (2023).

[12] R. Chaves, G. Moreno, E. Polino, D. Poderini, I. Agresti, A. Suprano, M. R. Barros, G. Carvacho, E. Wolfe, A. Canabarro, R. W. Spekkens, and F. Sciarrino, Causal Networks and Freedom of Choice in Bell's Theorem, *PRX Quantum* **2**, 040323 (2021).

[13] P. Bierhorst, E. Knill, S. Glancy, Y. Zhang, A. Mink, S. Jordan, A. Rommal, Y.-K. Liu, B. Christensen, S. W. Nam, M. J. Stevens, and L. K. Shalm, Experimentally generated randomness certified by the impossibility of superluminal signals, *Nature* **556**, 223 (2018).

[14] R. Colbeck and R. Renner, Free randomness can be amplified, *Nature Physics* **8**, 450 (2012).

[15] D. E. Koh, M. J. W. Hall, Setiawan, J. E. Pope, C. Marletto, A. Kay, V. Scarani, and A. Ekert, Effects of Reduced Measurement Independence on Bell-Based Randomness Expansion, *Physical Review Letters* **109**, 160404 (2012).

[16] Y. Liu, Q. Zhao, M.-H. Li, J.-Y. Guan, Y. Zhang, B. Bai, W. Zhang, W.-Z. Liu, C. Wu, X. Yuan, H. Li, W. J. Munro, Z. Wang, L. You, J. Zhang, X. Ma, J. Fan, Q. Zhang, and J.-W. Pan, Device-independent quantum random-number generation, *Nature* **562**, 548 (2018).

[17] L. Wooltorton, P. Brown, and R. Colbeck, Tight Analytic Bound on the Trade-Off between Device-Independent Randomness and Nonlocality, *Physical Review Letters* **129**, 150403 (2022).

[18] K. Horodecki, M. Winiewski, and S. Das, Fundamental limitations on the device-independent quantum conference key agreement, *Physical Review A* **105**, 022604 (2022).

[19] S. Das, S. Bäuml, M. Winiewski, and K. Horodecki, Universal Limitations on Quantum Key Distribution over a Network, *Physical Review X* **11**, 041016 (2021).

[20] X. Li, Y. Wang, Y. Han, and S.-N. Zhu, Effects of reduced measurements independence on self-testing, *Journal of Physics A: Mathematical and Theoretical* **55**, 495302 (2022).

[21] I. W. Primaatmaja, K. T. Goh, E. Y.-Z. Tan, J. T.-F. Khoo, S. Ghorai, and C. C.-W. Lim, Security of device-independent quantum key distribution protocols: A review, *Quantum* **7**, 932 (2023).

[22] U. Vazirani and T. Vidick, Fully Device-Independent Quantum Key Distribution, *Physical Review Letters* **113**, 140501 (2014).

[23] V. Zapatero, T. van Leent, R. Arnon-Friedman, W.-Z. Liu, Q. Zhang, H. Weinfurter, and M. Curty, Advances in device-independent quantum key distribution, *npj Quantum Information* **9**, 1 (2023).

[24] M. J. W. Hall, Local deterministic model of singlet state correlations based on relaxing measurement independence, *Physical Review Letters* **105**, 250404 (2010).

[25] G. Pütz, D. Rosset, T. J. Barnea, Y.-C. Liang, and N. Gisin, Arbitrarily Small Amount of Measurement Independence Is Sufficient to Manifest Quantum Nonlocality, *Physical Review Letters* **113**, 190402 (2014).

[26] G. Pütz and N. Gisin, Measurement dependent locality, *New Journal of Physics* **18**, 055006 (2016).

[27] M. Banik, M. R. Gazi, S. Das, A. Rai, and S. Kunkri, Optimal free will on one side in reproducing the singlet correlation, *Journal of Physics A: Mathematical and Theoretical* **45**, 205301 (2012).

[28] I. Šupić, J.-D. Bancal, and N. Brunner, Quantum nonlocality in presence of strong measurement dependence (2022), arXiv:2209.02337 [quant-ph].

[29] M. Kim, J. Lee, H.-J. Kim, and S. W. Kim, Tightest conditions for violating the Bell inequality when measurement independence is relaxed, *Physical Review A* **100**, 022128 (2019).

[30] A. S. Friedman, A. H. Guth, M. J. W. Hall, D. I. Kaiser, and J. Gallicchio, Relaxed Bell inequalities with arbitrary measurement dependence for each observer, *Physical Review A* **99**, 012121 (2019).

[31] J. R. Hance and S. Hossenfelder, What does it take to solve the measurement problem?, *Journal of Physics Communications* **6**, 102001 (2022).

[32] S. Donadi and S. Hossenfelder, Toy model for local and deterministic wave-function collapse, *Physical Review A* **106**, 022212 (2022).

[33] B. F. Toner and D. Bacon, Communication Cost of Simulating Bell Correlations, *Physical Review Letters* **91**, 187904 (2003).

[34] C. H. Brans, Bell's theorem does not eliminate fully causal hidden variables, *International Journal of Theoretical Physics* **27**, 219 (1988).

[35] M. J. W. Hall and C. Branciard, Measurement-dependence cost for Bell nonlocality: Causal versus retrocausal models, *Physical Review A* **102**, 052228 (2020).

[36] J. Gallicchio, A. S. Friedman, and D. I. Kaiser, Testing Bell's Inequality with Cosmic Photons: Closing the Setting-Independence Loophole, *Physical Review Letters* **112**, 110405 (2014).

[37] J. Handsteiner, A. S. Friedman, D. Rauch, J. Gallicchio, B. Liu, H. Hosp, J. Kofler, D. Bricher, M. Fink, C. Leung, A. Mark, H. T. Nguyen, I. Sanders, F. Steinlechner, R. Ursin, S. Wengerowsky, A. H. Guth, D. I. Kaiser, T. Scheidl, and A. Zeilinger, Cosmic Bell Test: Measurement Settings from Milky Way Stars, *Physical Review Letters* **118**, 060401 (2017).

[38] D. Rauch, J. Handsteiner, A. Hochrainer, J. Gallicchio, A. S. Friedman, C. Leung, B. Liu, L. Bulla, S. Ecker, F. Steinlechner, R. Ursin, B. Hu, D. Leon, C. Benn, A. Ghedina, M. Cecconi, A. H. Guth, D. I. Kaiser, T. Scheidl, and A. Zeilinger, Cosmic Bell Test Using Random Measurement Settings from High-Redshift Quasars, *Physical Review Letters* **121**, 080403 (2018).

[39] C. Wu, B. Bai, Y. Liu, X. Zhang, M. Yang, Y. Cao, J. Wang, S. Zhang, H. Zhou, X. Shi, X. Ma, J.-G. Ren, J. Zhang, C.-Z. Peng, J. Fan, Q. Zhang, and J.-W. Pan, Random Number Generation with Cosmic Photons, *Physical Review Letters* **118**, 140402 (2017).

[40] M.-H. Li, C. Wu, Y. Zhang, W.-Z. Liu, B. Bai, Y. Liu, W. Zhang, Q. Zhao, H. Li, Z. Wang, L. You, W. J. Munro, J. Yin, J. Zhang, C.-Z. Peng, X. Ma, Q. Zhang, J. Fan, and J.-W. Pan, Test of Local Realism into the Past without Detection and Locality Loopholes, *Physical Review Letters* **121**, 080404 (2018).

[41] N. D. Mermin, What's Wrong with these Elements of Reality?, *Physics Today* **43**, 9 (1990).

[42] N. D. Mermin, Simple unified form for the major no-hidden-variables theorems, *Physical Review Letters* **65**, 3373 (1990).

[43] A. Peres, Incompatible results of quantum measurements, *Physics Letters A* **151**, 107 (1990).

[44] J.-Å. Larsson, Loopholes in Bell inequality tests of local realism, *Journal of Physics A: Mathematical and Theoretical* **47**, 424003 (2014).

[45] T. M. Nieuwenhuizen, Is the Contextuality Loophole Fatal for the Derivation of Bell Inequalities?, *Foundations of Physics* **41**, 580 (2011).

[46] A. Khrennikov, Contextuality, Complementarity, Signaling, and Bell Tests, *Entropy* **24**, 1380 (2022).

[47] M. Kupczynski, Is the Moon There If Nobody Looks: Bell Inequalities and Physical Reality, *Frontiers in Physics* **8**, 10.3389/fphy.2020.00273 (2020).

[48] J. F. Clauser, M. A. Horne, A. Shimony, and R. A. Holt, Proposed experiment to test local hidden-variable theories, *Physical Review Letters* **23**, 880 (1969).

[49] T. N. Palmer, A local deterministic model of quantum spin measurement, *Proceedings of the Royal Society of London. Series A: Mathematical and Physical Sciences* **451**, 585 (1997).

**Appendix A: Symmetric random walk with an unequal probability of remaining still or moving left or right with step size 2**

We now consider the case of a symmetric random walk with a probability of  $\frac{1}{4}$  of moving left or right with step size 2:  $\Delta\lambda_1 = \Delta\lambda_2 = 2$  and a probability  $\frac{1}{2}$  of remaining still. The probability of adopting a particular value of  $\lambda_i$  at time  $-t$ , given the system has collapsed at measurement outcome (target)  $\lambda_i^\pm$  associated with the measurement setting  $\hat{n}_i$  at  $t = 0$ , is then expressed as:

$$P(\lambda_i | \lambda_i^\pm, \hat{n}_i)_{-t} = \sum_{N_r, N_l, N_s} \left(\frac{1}{4}\right)^{N_r} \left(\frac{1}{4}\right)^{N_l} \left(\frac{1}{2}\right)^{N_s} \frac{t!}{N_r! N_l! N_s!}, \quad (\text{A1})$$

subject to the restriction  $t = N_s + N_r + N_l$ , where  $N_r$  is the total number of times the system moves right and  $N_l$  the total number of times it moves left in a given time  $t$ .  $N_s, N_r$  and  $N_l$  can all take integer values between  $0 \rightarrow t$ . The possible values of  $\lambda_i$  would then be given by  $\lambda_i = \lambda_i^\pm + N_r - N_l$ . The expression in the sum in Eq. (A1) reflects that there may be multiple combinations of values of  $N_r, N_l$  and  $N_s$  that lead to the same value of  $\lambda_i$  and thus to compute the total probability of adopting the value  $\lambda_i$ , we must add these contributions together. The probability distribution over  $\lambda_1$  and  $\lambda_2$  can then be found through Eq. (12), since the random walks in each dimension are independent. We can calculate the additional term  $\mu$  in the Bell bound using Eq. (4).

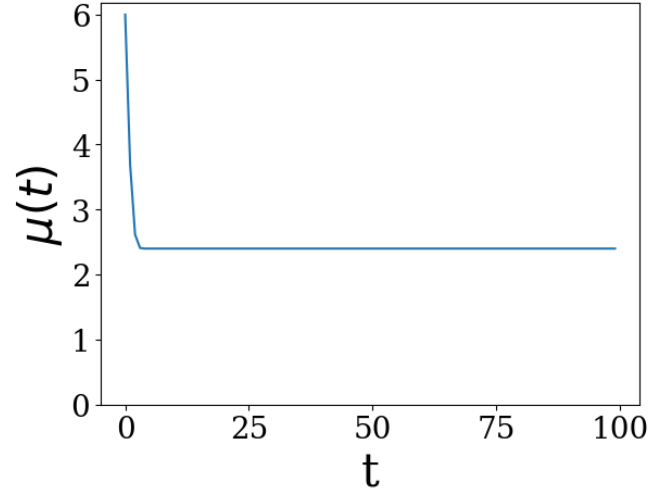


Figure 13. The evolution of the additional term  $\mu(t)$  where  $t$  is the time between when the system is measured and when it was prepared. The dynamics are such that there is a probability of  $\frac{1}{4}$  of moving left or right with step size 2:  $\Delta\lambda_1 = \Delta\lambda_2 = 2$  and a probability  $\frac{1}{2}$  of remaining still. The probabilities of arrival are  $P_{\pm\pm}^{\hat{a}, \hat{b}} = P_{\pm\pm}^{\hat{a}', \hat{b}} = P_{\pm\pm}^{\hat{a}'', \hat{b}'} = P_{\pm\mp}^{\hat{a}, \hat{b}'} = 0.45$  and  $P_{\pm\mp}^{\hat{a}, \hat{b}} = P_{\pm\mp}^{\hat{a}', \hat{b}} = P_{\pm\mp}^{\hat{a}'', \hat{b}'} = P_{\pm\pm}^{\hat{a}, \hat{b}'} = 0.05$ .

Figure 13 illustrates how the numerically calculated additional term  $\mu$  varies with time  $t$  for the aforementioned dynamics. It can be seen that the additional term decreases to a plateau at a value of around 2.4, where it remains, similarly to the dynamics of a symmetric random walk with equal probability of moving left or right by one spacing. At  $t = 100$ , the additional term remains nonzero, revealing that the conditioning of the probability distributions of the hidden variables on the chosen measurement setting persists.

Figure 14 depicts how the numerical  $2 + \mu_{num}$  (blue

dashes) and asymptotically calculated  $2 + \mu_{asym}$  (orange dots) additional term vary with  $C(\hat{a}, \hat{b})$ , and contrasted with the Bell bound on the CHSH parameter (green). The asymptotic value of the additional term is found in a similar way to that outlined in Section V. Here it appears to exactly match the numerically calculated value.

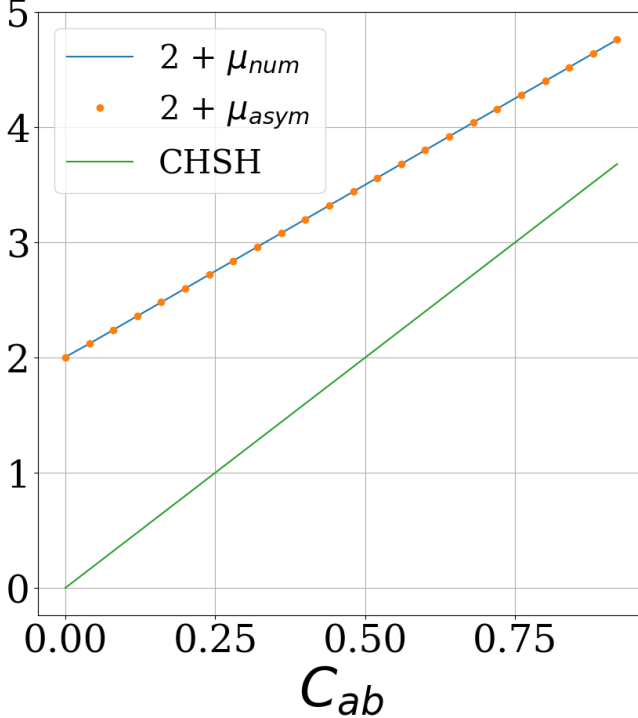


Figure 14. The new upper bound  $2 + \mu$  of the CHSH parameter for different values of the correlation function  $C(\hat{a}, \hat{b})$  for a symmetric random walk with point targets and a probability of  $\frac{1}{4}$  of moving left or right with step size 2 and a probability of  $\frac{1}{2}$  of remaining still.  $2 + \mu_{num}$  is calculated numerically at  $t = 10$  (blue dashes) and compared with the asymptotic value  $2 + \mu_{asym}$  (orange dots) and the corresponding Bell bound on the CHSH parameter (green). The probabilities of arrival form the same pattern as depicted in Figure 3.

Figure 15A) depicts how the probability distribution of the hidden variables varies for measurement settings (a)  $(\hat{a}, \hat{b})$  and b)  $(\hat{a}, \hat{b}')$ . It can be seen that the probability for odd-odd and even-even values of  $\lambda_1, \lambda_2$  is high in Figure 15A a) while in Figure 15A b) it is low. This difference between the distributions leads to an additional term that is high enough to account for Bell bound breaking correlations.

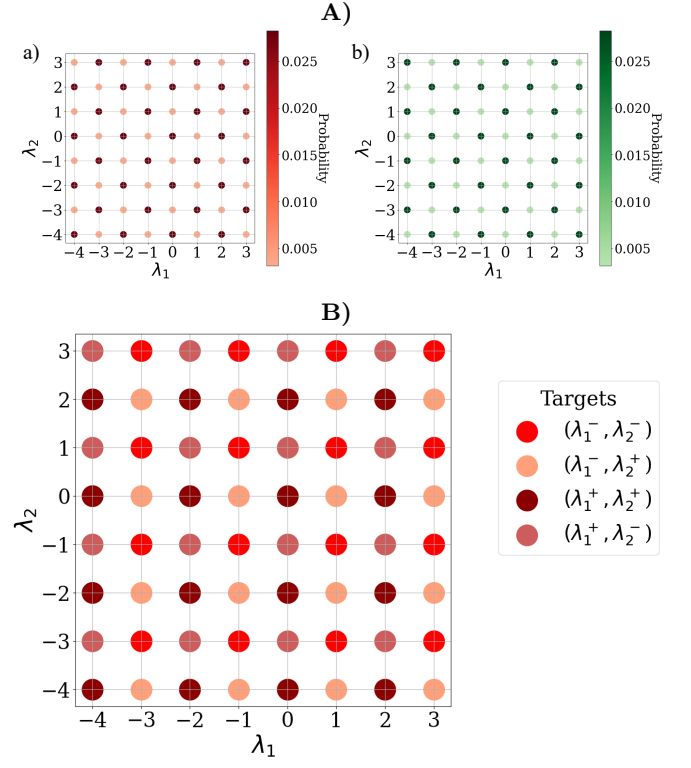


Figure 15. A) The evolution of the probability distribution of the hidden variables for measurement setting (a)  $(\hat{a}, \hat{b})$  and b)  $(\hat{a}, \hat{b}')$  at time  $t = 10$  and with probabilities of arrival  $P_{\pm\pm}^{\hat{a}, \hat{b}} = P_{\pm\pm}^{\hat{a}', \hat{b}'} = P_{\pm\mp}^{\hat{a}', \hat{b}'} = P_{\pm\mp}^{\hat{a}, \hat{b}'} = 0.45$  and  $P_{\pm\mp}^{\hat{a}, \hat{b}} = P_{\pm\mp}^{\hat{a}', \hat{b}'} = P_{\pm\mp}^{\hat{a}', \hat{b}'} = P_{\pm\pm}^{\hat{a}, \hat{b}'} = 0.05$ . B) The possible values of  $\lambda_1$  and  $\lambda_2$  associated with arrival at each of the four targets when  $\hat{a}$  and  $\hat{b}$  are chosen to be the measurement settings at  $t = 10$ .

Figure 15B) shows the possible values of  $\lambda_1$  and  $\lambda_2$  associated with arrival at each of the four targets for measurement setting  $(\hat{a}, \hat{b})$ . For example, only odd-odd values of  $\lambda_1, \lambda_2$  are associated with odd-odd targets, and similarly for the other targets. Only one of the four possible targets may be reached from a particular value of  $\lambda_1$  and  $\lambda_2$ , defined by their parity, such that basins of attraction to each target exist. This is why the dynamics in question are able to produce sufficiently different probability distributions for  $\lambda_1$  and  $\lambda_2$ , such as those depicted in Figure 15A), that can lead to a nonzero asymptotic additional term.

Note that this case is similar to that of the symmetric random walk dynamics with equal probabilities of moving left or right by one spacing, but the dynamics are such that at even and odd time-steps the possible values of  $\lambda_1$  and  $\lambda_2$  associated with an even-even target will both be even and those associated with an odd-even target will be odd and even respectively, where for the simpler dynamics this would only be the case when the time-step is even.

## Appendix B: Asymmetric random walk dynamics

In the main text as well as the preceding Appendix, we assumed symmetric random walk measurement dynamics for both hidden variables. We extend this to explore a random walk with an asymmetric step size for both variables: the step size when moving left is  $\Delta\lambda_l = 2$  whilst the step size when moving right is  $\Delta\lambda_r = 1$ . The possible values of  $\lambda_i$  would then be  $\lambda_i = \lambda_i^\pm + \Delta\lambda_r N_r - \Delta\lambda_l (t - N_r)$  where  $N_r$  is the total number of moves taken to the right for a given evolution pathway, taking integer values between 0 and  $t$ , and  $N_l = t - N_r$  is the total number of moves taken to the left.  $\lambda_i^\pm$  denotes the target (measurement outcome) for a given measurement setting  $\hat{n}_i$ . The probability of adopting the initial hidden variable value  $\lambda_i$  is then found using

$$p(\lambda_i | \lambda_i^\pm, \hat{n}_i)_{-t} = \frac{1}{2^t} \frac{t!}{(\lambda_i^\pm - 1)!(t + 1 - \lambda_i^\pm)!}, \quad (\text{B1})$$

and Eq. (12) can then be used to calculate the probability distributions. We implement periodic boundaries expressed by  $\lambda_{PB} = ((\lambda + \frac{9}{2}) \oplus 9) - \frac{9}{2}$  rather than  $\lambda_{PB} = ((\lambda + 4) \oplus 8) - 4$  used previously. The size of the boundary needs to be a multiple of three in order for the basins of attraction leading to the four targets in a given measurement situation not to mix.

Figure 16 illustrates how the additional term  $\mu(t)$  varies with time for the dynamics described above. Similarly to Figure 13, the additional term decreases until it reaches a plateau at a value of around 2.4, where it remains. It therefore takes a significant value even at asymptotic time.

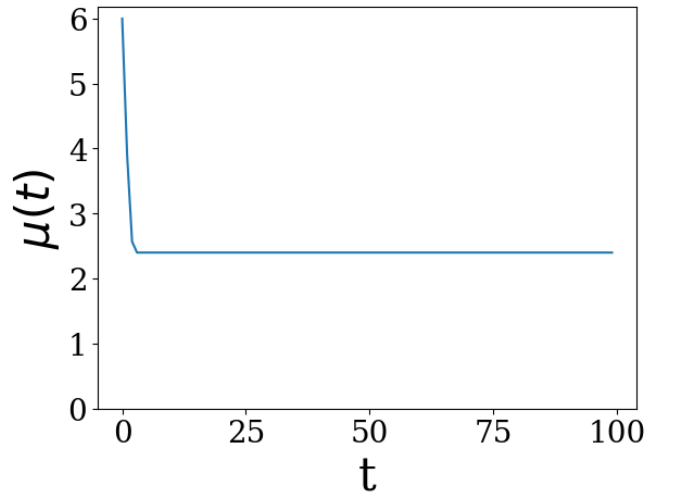


Figure 16. The evolution of the numerically calculated additional term  $\mu(t)$  where  $t$  is the time between when the system was measured and when it was prepared. The dynamics are such that there is an equal probability of moving left with step size 2 or right with step size 1. The probabilities of arrival are  $P_{\pm\pm}^{\hat{a},\hat{b}} = P_{\pm\pm}^{\hat{a}',\hat{b}} = P_{\pm\pm}^{\hat{a}',\hat{b}'} = P_{\pm\mp}^{\hat{a},\hat{b}'} = 0.45$  and  $P_{\pm\mp}^{\hat{a},\hat{b}} = P_{\pm\mp}^{\hat{a}',\hat{b}} = P_{\pm\mp}^{\hat{a}',\hat{b}'} = P_{\pm\pm}^{\hat{a},\hat{b}'} = 0.05$ .

Figure 17 depicts how the numerical  $(2 + \mu_{num})$  (blue dashes) and the analytical asymptotic value  $(2 + \mu_{asym})$  (orange dots) of the additional term, and the CHSH parameter (orange) depend on  $C(\hat{a}, \hat{b})$  for the dynamics specified above. The additional term appears to evolve in a similar manner to Figure 7.

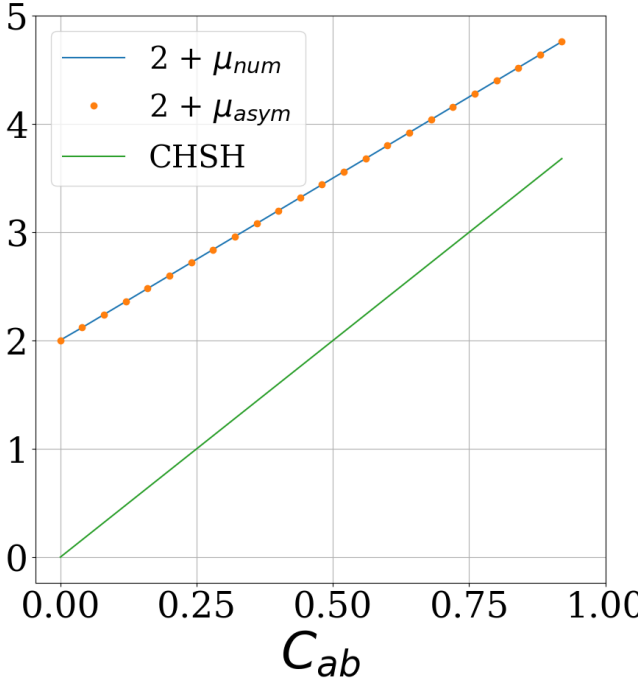


Figure 17. The new upper bound  $2 + \mu$  of the CHSH parameter for different values of the correlation function  $C(\hat{a}, \hat{b})$  for a asymmetric random walk with point targets and an equal probability of moving left with step size 2 and right with step size 1.  $2 + \mu_{num}$  is calculated numerically at  $t = 10$  (blue dashes) and compared with the asymptotic value of  $2 + \mu_{asym}$  (orange dots) and the corresponding value of the CHSH parameter (green). The probabilities of arrival form the same pattern as depicted in Figure 3, those with darker shades take the range of values:  $P_{\pm\pm}^{\hat{a}, \hat{b}} = P_{\pm\pm}^{\hat{a}', \hat{b}} = P_{\pm\pm}^{\hat{a}', \hat{b}'} = P_{\pm\mp}^{\hat{a}, \hat{b}'} = 0.25 - 0.48$  whilst those with the lighter shades take the range of values:  $P_{\pm\mp}^{\hat{a}, \hat{b}} = P_{\pm\mp}^{\hat{a}', \hat{b}} = P_{\pm\mp}^{\hat{a}', \hat{b}'} = P_{\pm\pm}^{\hat{a}, \hat{b}'} = 0.02 - 0.25$ .

Figure 18 (A) illustrates the probability distributions of the hidden variable for measurement settings a)  $(\hat{a}, \hat{b})$  and b)  $(\hat{a}', \hat{b})$ . Similar distributions to a) are found for  $\rho(\lambda_1, \lambda_2 | \hat{a}, \hat{b})$  and  $\rho(\lambda_1, \lambda_2 | \hat{a}', \hat{b}')$ . Similarly to the symmetric random walk case in Figure 6 (A), Figure 18 (A) shows a checkerboard of points of high and low probability. The values of  $\lambda_1$  and  $\lambda_2$  with high and low probability in a) are opposite to those in b), leading to a difference between  $\rho(\lambda_1, \lambda_2 | \hat{a}', \hat{b})$  and the other three probability distributions. Note that in the symmetric case,  $\rho(\lambda_1, \lambda_2 | \hat{a}, \hat{b}')$  had a different pattern of probability to the other three distributions, whereas in the asymmetric case,  $\rho(\lambda_1, \lambda_2 | \hat{a}', \hat{b})$  is the probability distribution that is the odd one out, as a result of the dynamics.

Unlike the symmetric case, there are values of  $\lambda_1$  and  $\lambda_2$  that have a probability of adoption of zero across all measurement situations at a given time-step and instead the values of  $\lambda_1$  and  $\lambda_2$  with non-zero probability are clustered in groups of four. Each possible value of  $\lambda$  has a cycle of three time-steps. For example, consider that at  $t = 1$ , 1 is one of the many possible values of  $\lambda$ . At

time-steps  $t = 2$  and  $3$ ,  $\lambda = 1$  is inaccessible and does not form one of the possible values of  $\lambda$ , but at  $t = 4, 8, 16\dots$  it will.

Figure 18 (B) depicts the different possible values of  $\lambda_1$  and  $\lambda_2$  for measurement setting  $(\hat{a}, \hat{b})$  leading to the four different targets. Similar plots are formed for  $\rho(\lambda_1, \lambda_2 | \hat{a}', \hat{b})$ ,  $\rho(\lambda_1, \lambda_2 | \hat{a}, \hat{b}')$  and  $\rho(\lambda_1, \lambda_2 | \hat{a}', \hat{b}')$ . Since for a given measurement situation, each target possesses a unique set of  $\lambda_1$  and  $\lambda_2$  values, unique basins of attraction must exist, leading to a significant value of the additional term in Figure 17. Note however, that unlike the symmetric case, the basins of attraction leading to a target are not defined by the parity of the target. In other words, there are values of  $\lambda_1$  and  $\lambda_2$  of all parities that can lead to an even-even target, and similarly for the other three targets. Nonetheless, the values of  $\lambda_1$  and  $\lambda_2$  leading to an even-even target, whilst not all even at an even time-step, will be different to the values of  $\lambda_1$  and  $\lambda_2$  leading to the other three targets. The same can be said for the other targets. There are therefore still two unique basins of attraction for  $\lambda_1$  and two for  $\lambda_2$ , leading to the targets in a given measurement situation.

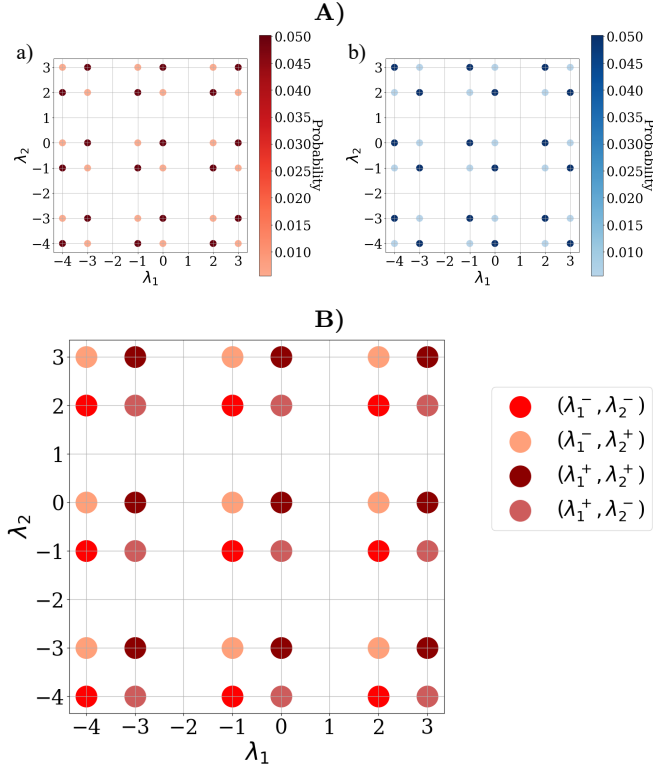


Figure 18. **A)** Probability distributions of the hidden variables  $\lambda_{1,2}$  for measurement settings a)  $(\hat{a}, \hat{b})$  b)  $(\hat{a}', \hat{b})$ , for an asymmetric random walk with step size 2 for moving left and 1 for moving right. Point targets were considered and an equal probability of moving left or right. The post-measurement outcome probabilities are  $P_{\pm\pm}^{\hat{a}, \hat{b}} = P_{\pm\mp}^{\hat{a}, \hat{b}} = P_{\mp\pm}^{\hat{a}', \hat{b}'} = P_{\mp\mp}^{\hat{a}', \hat{b}'} = 0.45$  and  $P_{\pm\mp}^{\hat{a}, \hat{b}} = P_{\pm\mp}^{\hat{a}', \hat{b}'} = P_{\mp\pm}^{\hat{a}', \hat{b}'} = P_{\mp\mp}^{\hat{a}, \hat{b}'} = 0.05$ , calculated at  $t = 10$ . **B)** Possible values of  $\lambda_1$  and  $\lambda_2$  leading to each of the four different targets  $(\lambda_1^\pm, \lambda_2^\pm)$  for measurement setting  $(\hat{a}, \hat{b})$ . The probabilities of arrival are  $P_{\pm\pm}^{\hat{a}, \hat{b}} = P_{\pm\mp}^{\hat{a}, \hat{b}} = P_{\mp\pm}^{\hat{a}', \hat{b}'} = P_{\mp\mp}^{\hat{a}', \hat{b}'} = 0.45$  and  $P_{\pm\mp}^{\hat{a}, \hat{b}} = P_{\pm\mp}^{\hat{a}', \hat{b}'} = P_{\mp\pm}^{\hat{a}', \hat{b}'} = P_{\mp\mp}^{\hat{a}, \hat{b}'} = 0.05$ , calculated at  $t = 10$ .